

Novel CK2-Specific Pt(II) Compound Reverses Cisplatin-Induced Resistance by Inhibiting Cancer Cell Stemness and Suppressing DNA Damage Repair in Non-small Cell Lung Cancer Treatments

Yuanjiang Wang,[§] Xinyi Wang,[§] Gang Xu, and Shaohua Gou*

Cite This: *J. Med. Chem.* 2021, 64, 4163–4178

Read Online

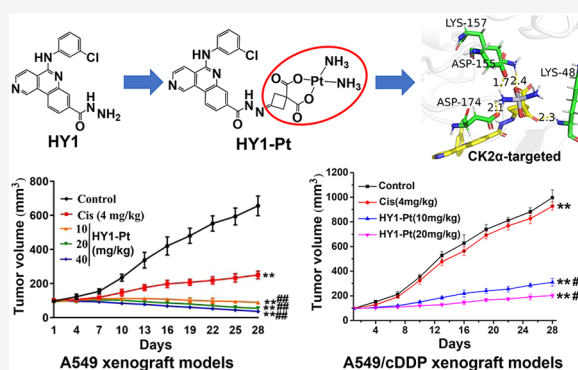
ACCESS |

Metrics & More

Article Recommendations

Supporting Information

ABSTRACT: Cancer stem cells (CSCs) have a pivotal impact in drug resistance, tumor metastasis, and progression of various cancer entities, including in non-small cell lung cancer (NSCLC). A CK2 inhibitor HY1 was found to show potent CSC inhibitory effects in A549 cells. By taking advantage of inherent CK2 specificity and CSC inhibition of HY1, a Pt(II) agent (HY1-Pt) was developed by conjugation of HY1 with an active Pt(II) unit to reverse cisplatin-induced resistance in A549/cDDP cell treatment. *In vitro* biological studies indicated that HY1-Pt can target CK2, suppress DNA damage repair, reinforce cellular accumulation of platinum, and reverse resistance apart from effectively inhibiting CSCs through Wnt/ β -catenin signal pathway in A549/cDDP cells. Significantly, HY1-Pt presented an acceptable pharmacokinetic behavior and exhibited higher tumor growth inhibitory efficacy than cisplatin either in A549 or A549/cDDP xenograft models with low toxicity. Overall, HY1-Pt is a promising drug candidate for NSCLC treatment.



1. INTRODUCTION

Lung cancer has become a serious public health issue, and its morbidity and mortality are increasing year by year, and it has become the first cause of death of malignant tumors in urban population of China.^{1,2} Non-small cell lung cancer (NSCLC) occupies almost 85% of all lung cancers. More serious, nearly 70% of all patients with NSCLC with locally advanced or metastatic disease need systemic therapy, but they have only a median survival time of about 18 months in the inoperable stage.³ There are several reasons that NSCLC is difficult to cure: (i) most of the patients are found to be in the middle or advanced-stage and those who have received front-line chemotherapy face fruitless treatments.⁴ (ii) Lung cancers have serious intratumoral heterogeneity. According to statistics, as many as 63% of NSCLC patients contain more than one histological subtype.^{5,6} (iii) The intrinsic and/or acquired drug resistance from traditional drugs or targeted tyrosine kinase inhibitors is still a major problem in clinic. So, new agents are urgently needed to overcome drug resistance.⁷

Lung cancer intratumoral heterogeneity is driven by subpopulations of tumor cells termed as cancer stem cells (CSCs).⁸ CSCs, a small subset of cancer cells, can differentiate into different phenotypes with the ability of continuous self-renewal, differentiation, and highly tumorigenic subpopulation.⁹ Unlike the bulk of tumor cells, CSCs are critically involved in tumorigenesis, tumor recurrence, cancer invasion, and metastasis. Moreover, mounting evidence suggests that

CSCs in the quiescent phase can lead to primary and acquired drug resistance through DNA self-repair, ABC transporters, and mutation such as point mutation, gene mutation, and gene amplification, responsible for the failure of many cancer treatments.^{10,11} Therefore, development of targeted chemotherapeutic drugs to abrogate CSCs is a key task in lung cancer research and clinical application.

Multi-regimen chemotherapy for NSCLC usually involves the combination of platinum-based drugs like cisplatin and other drugs with different mechanisms of action. According to the statistics, more than half of chemotherapy regimens contain platinum-based antitumor drugs.^{12–15} However, non-specificity and drug resistance in addition to toxicity are still major inevitable barriers for their clinical use.¹⁶ The great success and drawback of cisplatin have encouraged researchers to conduct more in-depth and detailed studies on its mechanism of action, attempting to achieve novel platinum-based drugs with higher efficiency, lower toxicity, and better reversal of resistance. So far, the mechanism of cisplatin resistance is recognized as follows: (i) decreased intracellular

Received: January 16, 2021

Published: March 30, 2021



Scheme 1. Synthesis of HY1 and HY1-Pt

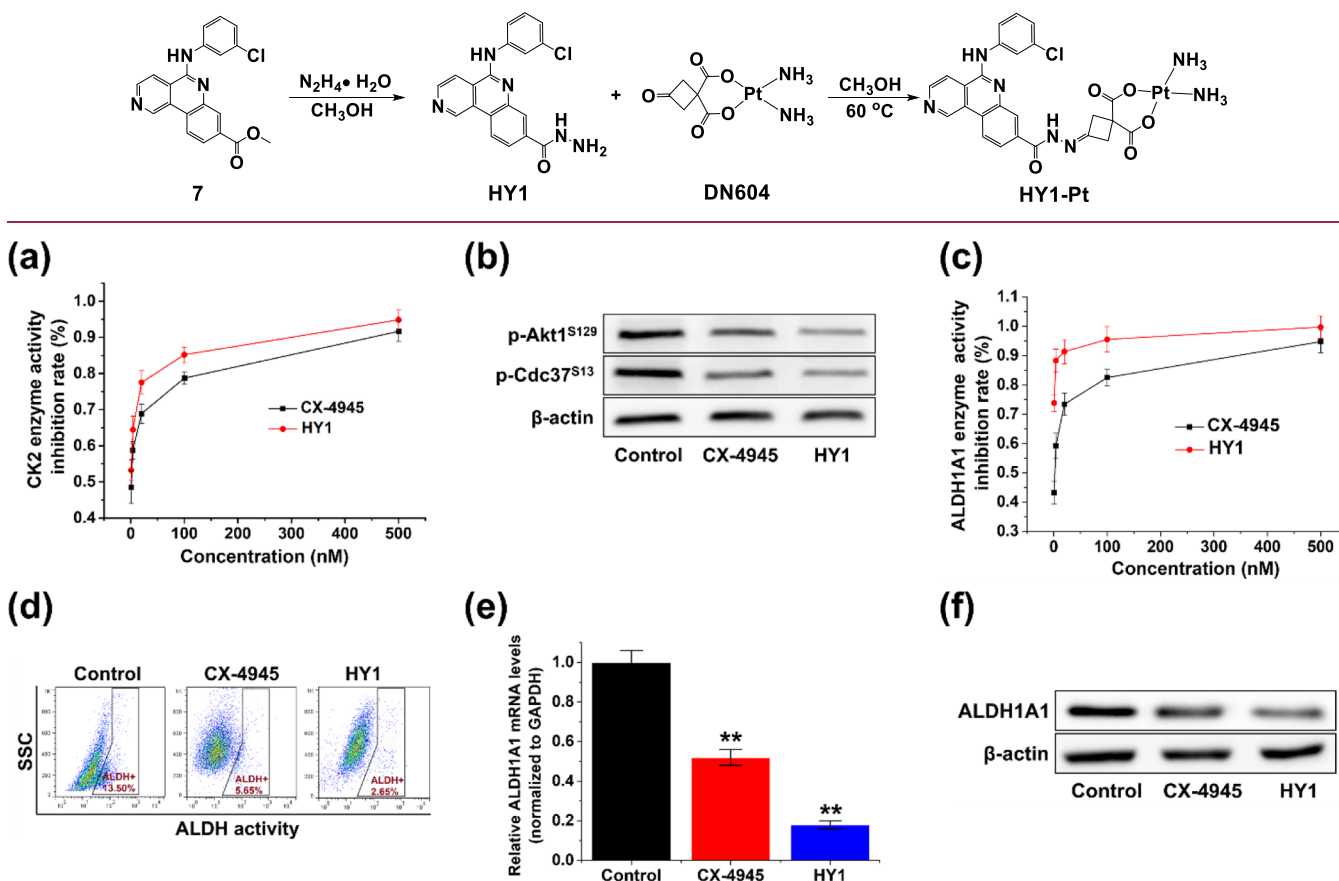


Figure 1. Inhibitory activity of HY1 on CK2 and its effect on A549 cell stemness. (a) Inhibition rate curves of HY1 and CX-4945 on CK2 enzyme activity. (b) Western blot analysis on the specific CK2 phosphorylation targets: phosphorylation of the Akt1 serine 129 and Cdc37 serine 13 in A549 cells after treatment with CX-4945 and HY1 at 20 μ M, respectively, for 24 h. (c) Inhibition rate curves of HY1 and CX-4945 on ALDH1A1 enzyme activity. (d) Percentage of ALDH⁺ cells in A549 cells after treatment with CX-4945 and HY1 at 20 μ M, respectively, for 24 h. (e) ALDH1A1 mRNA levels after treatment with CX-4945 and HY1 at 20 μ M, respectively, for 24 h in A549 cells. (f) ALDH1A1 protein levels treated with CX-4945 and HY1 at 20 μ M, respectively, for 24 h in A549 cells. Data were obtained via using students' *T*-test, *n* = 3 per group, Error bars = SD, asterisk indicate statistically significant differences, ***P* < 0.01, vs control.

platinum accumulation, (ii) detoxification of platinum ions by sulfhydryl molecules, and (iii) increased DNA damage repair levels.^{17–19} Besides, there are also other factors that may have impacts on the mechanism of drug resistance including DNA hypermethylation, histone modification, and chromatin structure changes.²⁰

Protein kinase CK2 plays a notable role in various essential and pathological biological processes.^{21–23} It has been proven that CK2 has more than 300 phosphorylated substrates, which is one of the most pleiotropic proteins in eukaryotic systems.^{24,25} CK2 is overexpressed in multiple tumors and rated as one of the most promising targets for treating many types of cancer and some life-threatening diseases.²⁶ Much significantly, CK2 can play a pivotal regulatory role in DNA damage repair and cancer stemness by Hedge-hog/Gli1, Wnt/ β -catenin, NF- κ B and PI3K, and so forth.^{27–29} In addition, CK2 inhibition also causes an increased uptake of known drugs in multidrug-resistant cells.^{30–33}

Notably, there has been a report that CK2 α positively regulates the population of CD44⁺/CD24⁻ and the transcriptional activity of Notch1, which is concerned in the maintenance of CSCs.³⁴ As CX-4945 is the sole small molecule CK2 inhibitor in phase I/II clinical trials,^{35–37} we

derived a hydrazide compound (HY1) upon the framework of CX-4945, which was found to exhibit potent capability of inhibiting cancer cell stemness. By taking the advantage of inherent CK2 specificity and CSC inhibition of HY1, a novel Pt(II) compound was developed by conjugation of HY1 with an active Pt(II) unit as an antitumor agent, attempting to enhance antitumor efficacy and overcome cisplatin-induced resistance by targeting CK2, suppressing DNA damage repair and inhibiting cancer cell stemness for the first time.

2. RESULTS AND DISCUSSION

2.1. Preparation of HY1 and HY1-Pt. CX-4945 and compound 7 were synthesized in accordance with the procedures reported previously (Scheme S1).²⁵ The synthetic route of HY1 and HY1-Pt is shown in Scheme 1. Treatment of compound 7 with hydrazine hydrate in refluxing methanol afforded HY1 which precipitated from the reaction mixture upon cooling. Direct condensation between HY1 with DN604, a known antitumor Pt(II) agent,³⁸ resulted in the formation of HY1-Pt. The resulting compounds were confirmed by ¹H, ¹³C NMR, and HR electrospray ionization-mass spectrometry (ESI-MS) spectroscopy with purity over 95% determined by RP-HPLC (see also the Supporting Information).

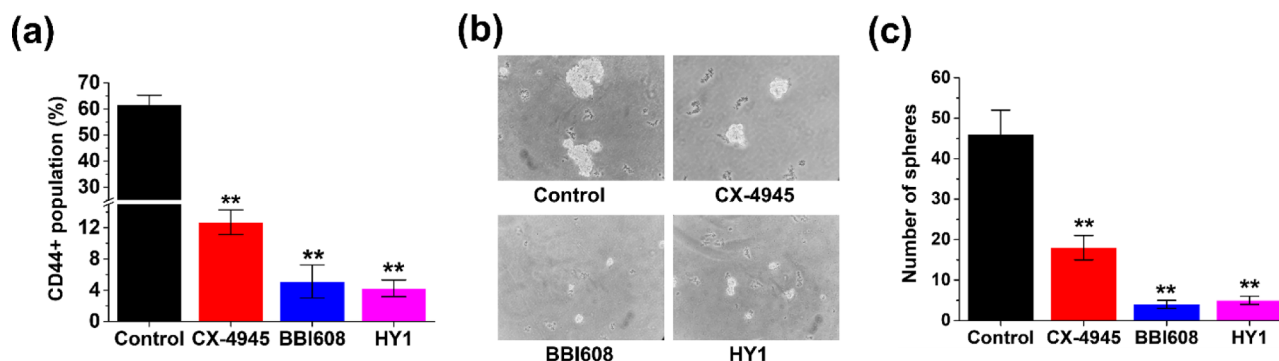


Figure 2. Study on the effect of HY1 on the expression of intracellular CD44⁺ and the formation of tumorsphere in A549 cells. (a) Statistics of the experimental results in Figure S1, and the proportion of CD44⁺ subsets in A549 cells treated with CX-4945, BBI608, and HY1 at 20 μ M, respectively, for 24 h were statistically analyzed. (b) Morphological image and (c) the number of A549 cells tumorsphere treated with CX-4945, BBI608, and HY1 at 10 μ M, respectively. Error bars = SD ($n = 3$), ** $P < 0.01$.

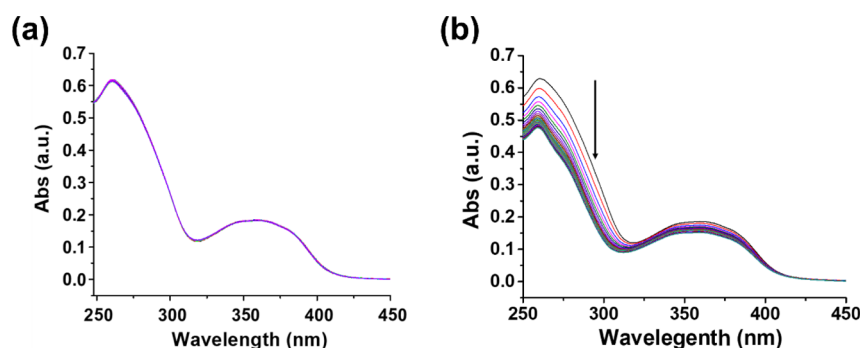


Figure 3. Stability of HY1-Pt in HEPES buffer at pH 7.4 and 6.0 measured by UV-vis. (a) Stability of HY1-Pt in HEPES buffer (pH = 7.4) containing 2% DMF was recorded via time-dependent UV-vis spectra (scan every 30 min for a total of 24 times) at 37.0 $^{\circ}$ C. (b) Stability of HY1-Pt in HEPES buffer (pH = 6.0) containing 2% DMF was recorded via time-dependent UV-vis spectra (scan every 10 min for 12 h) at 37.0 $^{\circ}$ C.

2.2. Inhibitory Activity of HY1 on CK2 and Its Effect on A549 Cells Stemness.

Since HY1 and CX-4945 share the same scaffold of benzo[*c*][2,6]naphthyridine, we explored whether HY1 retained the CK2 inhibitory activity of its parent compound, CX-4945. Thus, the human CK2 assay kit and the antibodies of the specific phosphorylation targets of CK2 were used to evaluate the activity of HY1 with CX-4945 as the positive control. As illustrated in Figure 1a, HY1 showed dose-dependent inhibition of CK2 with a higher IC_{50} value than CX-4945. Besides, HY1 also strongly inhibited the phosphorylation of Akt1 serine 129 and Cdc37 serine 13, two specific phosphorylation targets of CK2 (Figure 1b). These results indicated that HY1 maintained the inhibitory activity of the parent compound against CK2, even exhibiting slightly stronger activity than CX-4945.

As CK2 α can regulate the population of CD44⁺/CD24⁻ involved in stem cell maintenance,³⁴ we studied the inhibitory effect of HY1 on cancer cell stemness as well. Aldehyde dehydrogenases (ALDHs) are a superfamily of detoxifying enzymes that are overexpressed in various cancers.³⁹ Increasing expression of ALDHs, especially ALDH1A1, in a number of malignancies and CSCs are closely related to poor prognosis, aggressiveness, and drug resistance in cancer chemotherapy. Growing lines of evidence prove that ALDH1A1 plays a significant role in tumors and CSCs except for a biomarker of CSCs and a predictor of the prognosis.⁴⁰ As shown in Figure 1c, HY1 shows the potent inhibition on ALDH1A1 ($IC_{50} = 0.09 \pm 0.01 \mu$ M), which is 18.8-fold as much as that of CX-

4945 ($IC_{50} = 1.69 \pm 0.14 \mu$ M). The result indicated that HY1 had strong inhibitory activity on ALDH1A1 enzyme.

ALDH1A1 has been confirmed to play a notable effect in maintaining the stemness of A549 cells and is expressed preferentially.⁴¹ Therefore, in A549 cells, we hypothesize that ALDH1A1 has an important effect in facilitating the toxicological mechanism of HY1. First, the Aldefluor Assay was selected to determine the proportion of ALDH⁺ subsets in A549 cells. As shown in Figure 1d, the subpopulation of the ALDH⁺ cells were strongly reduced from 13.50 to 2.65% after treatment with HY1, stronger than that treated with CX-4945 (5.65%). Besides, as shown in Figure 1e, the transcriptional levels of ALDH1A1 in A549 cells presented a conspicuous decrease after being treated with HY1 at 20 μ M for 24 h. Meanwhile, the effect of HY1 on the expression of ALDH1A1 in A549 cells was also explored by western blot. As shown in Figure 1f, as expected, HY1 can also down-regulate the expression of ALDH1A1 in A549 cells, stronger than CX-4945.

CD44⁺ is a cell surface protein, which can interact with a variety of growth factors secreted, extracellular matrix, components, and cytokines by cells present in the tumor microenvironment.⁴² Therefore, CD44⁺ has also been identified as a marker for CSCs in a variety of tumors. In order to study the action of HY1 on cancer cell stemness further, the expression of CD44⁺ in A549 cells treated with HY1 was determined by flow cytometry using CX-4945 and BBI608 as positive controls. BBI608, currently in phase II/III clinical trials, is a STAT3 inhibitor which can potentially inhibit

Table 1. Cytotoxicity Profiles of HY1-Pt and Related Samples against A549 and A549/cDDP Cells

cell	IC ₅₀ (μM)						FI ^b
	CX-4945	HY1	HY1-Pt	cisplatin	DN604	DN604/HY1	
A549	22.39 ± 2.04	18.16 ± 2.21	5.10 ± 0.48	4.05 ± 0.30	16.93 ± 1.35	16.76 ± 1.32	0.79
A549/cDDP	25.08 ± 2.34	17.03 ± 1.02	4.84 ± 1.38	28.12 ± 1.71	48.56 ± 4.60	18.90 ± 1.65	5.81
RF ^a			0.95	6.94	2.86	1.12	

^aRF (resistant factor) = IC₅₀ (A549/cDDP)/IC₅₀ (A549). ^bFI (fold increase) = IC₅₀ (cisplatin)/IC₅₀ (HY1-Pt).

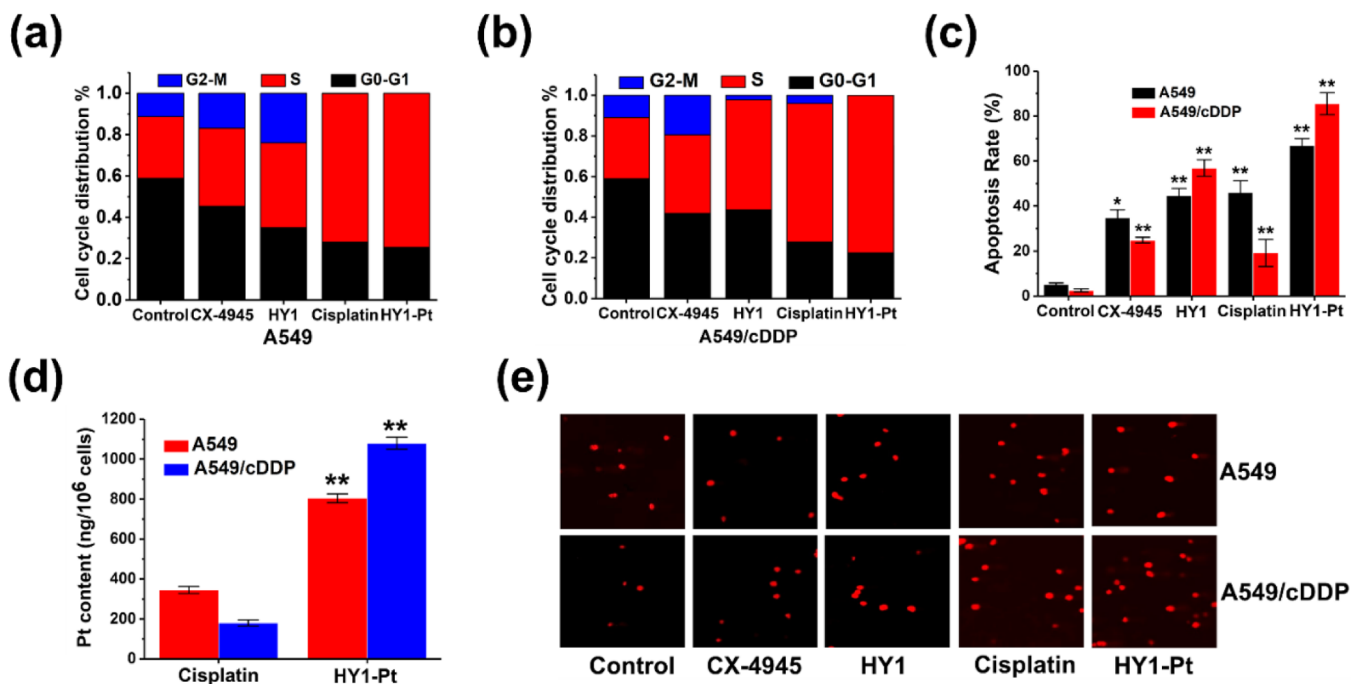


Figure 4. Cellular responses of CX-4945, HY1, cisplatin, and HY1-Pt in A549 and A549/cDDP cells. Statistics of the results of cell cycle arrest in Figure S3. Cell cycle arrest distributions of (a) A549 and (b) A549/cDDP cells were detected by flow cytometry after treatment with the tested compounds at 20 μM, respectively, for 24 h. (c) Statistics of the results of apoptosis in Figure S4. A549 and A549/cDDP cells were treated with the tested compound at 20 μM, respectively, for 24 h, and then, the apoptosis of the cells was detected by flow cytometry. (d) Intracellular accumulation of platinum in A549 and A549/cDDP cells was detected by ICP-MS after treatment with cisplatin and HY1-Pt at 20 μM, respectively, for 24 h. (e) Representative images of nuclei from comet assays. A549 and A549/cDDP cells were treated with the tested compounds at 20 μM, respectively, for 12 h. Error bars = SD ($n = 3$), * $P < 0.05$, ** $P < 0.01$.

the expression of the stemness gene, block the formation of tumorsphere, and kill CSCs isolated from multifarious cancer types.^{43,44} As shown in Figure 2a (see also the Supporting Information, Figure S1), the proportion of CD44⁺ subsets in A549 cells was 61.8%, which is in accordance with other reports.⁴⁵ HY1 showed an extremely strong inhibitory effect on CD44⁺ with an inhibition rate of 93.17%, higher than BBI608 (91.73%) or CX-4945 (79.45%). In addition, the function of HY1 on stemness phenotypes in A549 cells was also investigated. The cells were cultured in a three-dimensional microenvironment without or with CX-4945, BBI608, and HY1 for 24 h to detect their capability of tumorsphere formation. After the following 10-day treatment, the number of multicellular tumorsphere formed was counted. A549 tumorsphere cells treated with HY1 displayed reduced sphere sizes and numbers as compared to those treated with CX-4945, indicating that the inhibitory effect of HY1 was comparable to that of BBI608 (Figure 2b,c). Based on the above study, we assure that HY1 is a bifunctional molecule that inhibits both CK2 and cancer cell stemness.

2.3. Stability and Physicochemical Properties of HY1-Pt. Initially, the stability of HY1-Pt in HEPES buffer (0.25 M)

at pH 7.40 was studied via RP-HPLC and UV-vis at 37 °C. It was observed that HY1-Pt maintained its integrity after 12 h under the condition (Figures 3a and S2a). However, HY1-Pt was found to disassociate slowly by the hydrazine bond-breaking to yield HY1 under the tumor acidic microenvironment (pH = 6.0) (Figures 3b and S2b). As the lipid-water partition coefficient and LLE of a compound directly affects the absorption *in vivo*, the log $P_{o/w}$ value of HY1-Pt was measured as -0.031, and its LLE values were 5.301 and 5.351 in A549 and A549/cDDP cells, respectively, hinting that HY1-Pt may have good absorption and penetration according to Lipinski's rules.⁴⁶

2.4. In Vitro Cytotoxicity. Cytotoxicity of HY1 and HY1-Pt as well as a physical mixture of equimolar DN604 and HY1 against A549 (sensitive to cisplatin) and A549/cDDP (resistant to cisplatin) cells was evaluated via MTT assay using CX-4945, cisplatin, and DN604 as the positive drugs. As shown in Table 1, cisplatin displayed the most potent anticancer activity against A549 cells, while presented the weakest activity against cisplatin-resistant A549/cDDP cells among the measured compounds. Notably, HY1-Pt had cytotoxicity nearly as potent as cisplatin in A549 cells, but

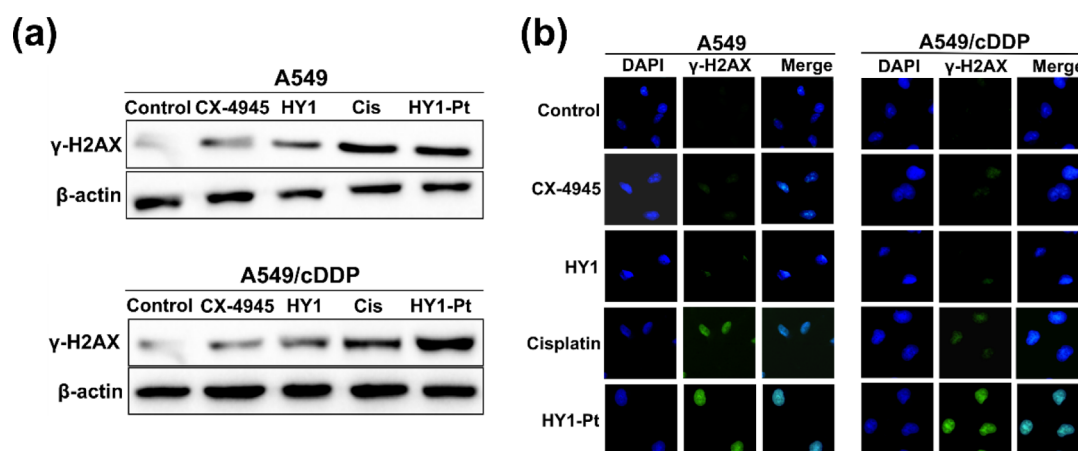


Figure 5. Analysis of the γ H2AX expression in A549 and A549/cDDP cells. (a) Expression of γ H2AX in two cell lines was analyzed by western blot after treatment with CX-4945, HY1, cisplatin (cis), and HY1-Pt at 20 μ M, respectively, for 24 h. (b) γ H2AX foci in two cell lines were determined via immunofluorescence staining after treatment with CX-4945, HY1, cisplatin, and HY1-Pt at 20 μ M, respectively, for 12 h.

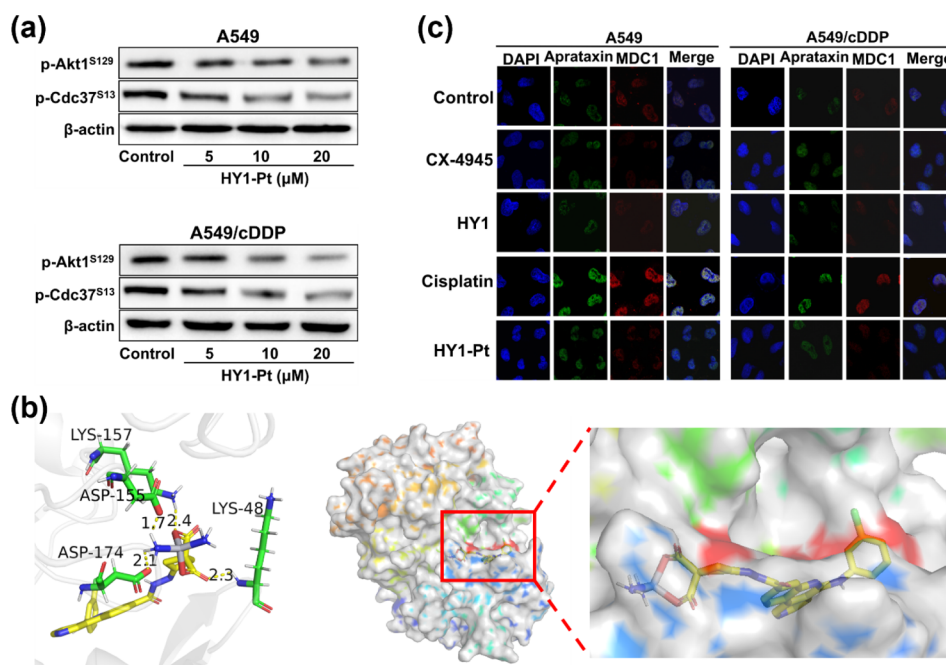


Figure 6. Investigation on the inhibition of HY1 on CK2 and DNA damage repair. (a) Western blotting assay on the expression of p-Akt1^{S129} and p-Cdc37^{S13} in either A549 or A549/cDDP cells after treatment with different concentrations of HY1-Pt for 24 h. (b) HY1-Pt is docked into the hydrophobic pocket of CK2 α protein (PDB ID: 6isj) utilizing Autodock. Amino acid residues that may be involved in the binding are labeled, and the yellow dashed indicate the hydrogen bond interaction. (c) The co-localization of MDC1/Aprataxin and the damaged DNA in either A549 or A549/cDDP cells were detected by immunofluorescence technique after treatment with CX-4945, HY1, cisplatin, and HY1-Pt at 20 μ M for 24 h.

the cytotoxicity of HY1-Pt to A549/cDDP cells was 5.81-fold higher than cisplatin with a RF (resistant factor) value of 0.95. It was noticed that DN604 and its physical mixture with HY1 showed almost the same cytotoxicity toward A549 cells. Even though the physical mixture showed 2.57-fold stronger cytotoxicity than DN604 against A549/cDDP cells, its activity was 3.90 times weaker than HY1-Pt. Based on the above results, HY1-Pt as well as its parent compounds CX-4945 and HY1 was also used to treat different cancer cells and human normal hepatocytes for comparison. As shown in Table S2, HY1-Pt exhibited more potent activity than HY1 and CX-4945 against these cancer cells. Significantly, HY1-Pt had the lowest toxicity to LO2 cells among the measured compounds. These results show that HY1-Pt exhibits strong inhibitory

activity against these cancer cells, especially cisplatin-mediated drug-resistant cancer cells.

2.5. Cellular Responses. In view of the *in vitro* anti-proliferation behavior of HY1-Pt on both A549 and A549/cDDP cells, its mechanisms of action were investigated. These two cancer cells were incubated with CX-4945, HY1, cisplatin, and HY1-Pt at 20 μ M for 24 h for studying cell arrest and apoptosis. As shown in Figure 4a,b (see also the Supporting Information, Figure S3), in either A549 or A549/cDDP cells, cisplatin arrests the cell cycle in the S phase, which is in accordance with other reports.⁴⁷ Notably, HY1-Pt arrests the cell cycle also in the S phase, similar to cisplatin. Meanwhile, both A549 and A549/cDDP cells are highly sensitive to HY1-Pt with apoptotic percentages from 66.9 to 85.5%, much more

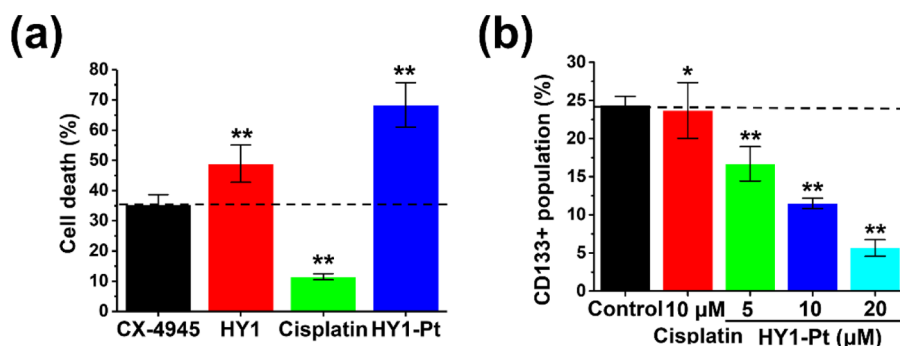


Figure 7. Study on the inhibitory effect of the tested compounds on A549/cDDP^{CD44}^{bright} and its intracellular CD133. (a) Mortality rate of A549/cDDP^{CD44}^{bright} cells incubated with CX-4945, HY1, cisplatin, and HY1-Pt at 20 μ M, respectively, for 24 h. (b) Expression of CD133 is analyzed in A549/cDDP^{CD44}^{bright} cells by flow cytometry. Error bars = SD ($n = 3$), * $P < 0.05$, ** $P < 0.01$.

effectively than cisplatin from 46.1 to 19.2% (Figures 4c and S4). To evaluate the high cytotoxicity of HY1-Pt, the cellular accumulation of Pt in A549 and A549/cDDP cells were determined via ICP-MS after being treated with HY1-Pt at 20 μ M for 12 h, using CX-4945 as a positive control. Significantly, the Pt accumulation of HY1-Pt in A549 and A549/cDDP cells is 2.33 and 6.00 times as much as that of cisplatin, respectively (Figure 4d). As anticipated, the Pt amount of cisplatin in resistant to cisplatin cells is less than that in sensitive to cisplatin cells, however, that of HY1-Pt in cisplatin resistant cells is greater than in cisplatin sensitive cells with an increasing fold of 1.34. The increased Pt content would promote DNA damage in cancer cells. As shown in Figure 4e, HY1-Pt produces longer length tails than cisplatin in these two cancer cells in a comet assay, while CX-4945 and HY1 display weaker DNA interactions than two Pt(II) agents. Based on the above, HY1-Pt has been proved to be capable of effectively promoting cellular accumulation of platinum, seriously causing DNA damage and largely inducing programmed cell death, exhibiting better antitumor activity than cisplatin in the cells either sensitive or resistant to cisplatin.

2.6. Study on the Expression of γ -H2AX. There are several kinds of DNA damage, such as base modification, in chain and link-crosslinking, single-strand (SSBs) and double-strand (DSBs) breaks, among which DSBs are considered to be the most serious damage to DNA. Since the occurrence of γ -H2AX is closely related to DSBs in a one-to-one correspondence, γ -H2AX appears an important indicator to detect DSBs in cells.^{48,49} Western blot, flow cytometry, and immunofluorescence techniques were used to detect the expression of γ -H2AX in either A549 or A549/cDDP cells. As illustrated in Figure 5a, HY1-Pt can promote the phosphorylation of H2AX in two cell lines more than cisplatin, especially in A549/cDDP cells. Besides, the results showed that cisplatin caused some DSBs in A549 cells, but such a damage effect obviously decreased in A549/cDDP cells. In contrast, HY1-Pt caused DSBs in A549 cells at a higher degree than that of cisplatin. Assessments of the γ H2AX expression by flow cytometry further verified that HY1-Pt could lead to severe DSBs in both A549 and A549/cDDP cells, whose effect was obviously higher than cisplatin (Figure S5). Furthermore, as shown in Figure 5b, HY1-Pt also caused more serious DSBs in A549/cDDP cells with stronger fluorescence intensity than that in A549 cells.

2.7. Investigation on the Inhibition of HY1-Pt on CK2 α and DNA Damage Repair. Since CK2 can be used as a key director in DNA damage repair and cancer cell stemness,

we explored whether HY1-Pt retained the CK2 inhibitory activity of HY1.^{27,28} As illustrated in Figure S6, HY1-Pt showed dose-dependent inhibition of CK2 enzyme activity, and its IC₅₀ was up to 1.14 \pm 0.24 nM. In addition, in either A549 or A549/cDDP cells, HY1-Pt can inhibit the phosphorylation of Akt1 serine 129 and Cdc37 serine 13 in a dose-dependent manner (Figure 6a). The potent inhibition of HY1-Pt on CK2 prompted us to further explore the binding mode between HY1-Pt and CK2 α protein through molecular docking. The template of the co-crystal structure of CK2 α complexed with CX-4945 (PDB ID: 6isj) was used. As shown in Figure 6b, the entire CK2 α molecular structure is completely wrapped in the CK2 α active cavity. In addition, the hydrogen atoms on the amino group act as hydrogen bond donors form hydrogen bonds with ASP-174 and ASP-155 residues, respectively, while the carbonyl and oxygen atoms in the ester bond act as hydrogen bond receptors to form hydrogen bonds with LYS-157 and LYS-48 residues, respectively. These four hydrogen bonds firmly rivet HY1-Pt in the active cavity of CK2 α with the lowest binding energy of -11.21 kcal/mol. These results prove that the hybrid of HY1 into DN604 makes HY1-Pt not only maintain the cytotoxicity of the active Pt(II) unit but also keep the ability of CX-4945 to target and inhibit CK2 α .

Mediator of DNA damage checkpoint 1 (MDC1) is an important protein involved in the DSB response pathway.⁵⁰ Using immunofluorescence technique, we checked MDC1 to explore whether HY1-Pt can inhibit DNA damage repair while promoting DNA damage. As shown in Figure 6c, HY1-Pt leads to dramatic reduction in co-localization of MDC1/apratinaxin and the damaged DNA compared with cisplatin in either A549 or A549/cDDP cells, demonstrating that HY1-Pt can suppress extensive DNA damage repair via inhibiting CK2 compared with cisplatin.

2.8. Investigation on the Inhibition of A549/cDDP^{CD44}^{bright} Cells. The expression of CSC surface antigens plays a key role in invasiveness, promoting cancer recurrence.⁵¹ In solid cancer, CSCs were defined based on CD44 expression by flow cytometry as CD44^{bright} population.⁵² In order to further investigate the inhibitory activity and mechanism of HY1-Pt on CSCs, CD44^{bright} population cells in A549/cDDP were sorted by a flow cytometer. First, using CX-4945, HY1 and cisplatin as positive controls, the inhibition rate of HY1-Pt to A549/cDDP^{CD44}^{bright} cells was detected by MTT assay. As shown in Figure 7a, HY1-Pt maintained a high sensitivity to A549/cDDP^{CD44}^{bright} cells with an inhibition rate of 68.36%, much higher than that of cisplatin (11.47%). In addition, the

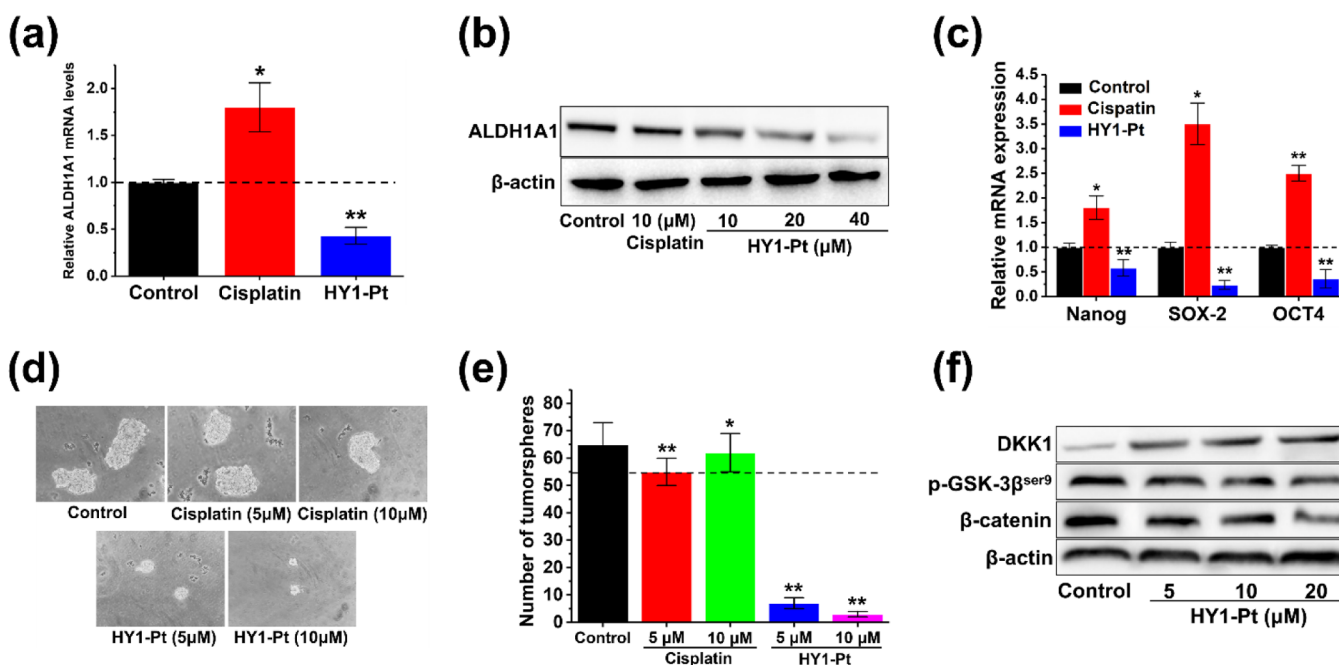


Figure 8. Study on A549/cDDP^{CD44}^{bright} cells. (a) qRT-PCR patterns of the ALDH1A1 in A549/cDDP^{CD44}^{bright} cells treated with cisplatin and HY1-Pt at 20 μM. (b) Expression of the ALDH1A1 in A549/cDDP^{CD44}^{bright} cells was explored by western blot after treatment with 10 μM cisplatin and HY1-Pt at concentrations of 10, 20, and 40 μM, respectively, for 24 h. (c) qRT-PCR patterns of the stem cell genes Nanog, SOX2, and OCT4 in A549/cDDP^{CD44}^{bright} cells treated with cisplatin and HY1-Pt at 20 μM, respectively. (d) Morphological observation and (e) the number of A549/cDDP^{CD44}^{bright} cells tumorsphere treated with cisplatin and HY1-Pt at two doses (5 and 10 μM), respectively. (f) Expression of DKK1, p-GSK-3β^(ser9), and β-catenin in A549/cDDP cells was explored by western blot after treatment with HY1-Pt at concentrations of 10, 20, and 40 μM, respectively, for 24 h. Error bars = SD (*n* = 3), **P* < 0.05, ***P* < 0.01.

expression of CSC surface antigens CD133⁺ in A549/cDDP^{CD44}^{bright} cells was 24.37%, which was 7.25 times higher than that in A549/cDDP cells (Figure S7). Notably, HY1-Pt also showed dose-dependent inhibition effects, and the inhibition rate reached 76.78% at 20 μM. In contrast, cisplatin had hardly significant inhibitory activity (Figure 7b).

The effect of HY1-Pt on ALDH1A1 expression in A549/cDDP^{CD44}^{bright} cells was also investigated. As expected, the transcriptional levels of ALDH1A1 showed a remarkable decrease in A549/cDDP^{CD44}^{bright} cells after being treated with HY1-Pt at 20 μM for 24 h. However, at the same dose, cisplatin promoted the expression of ALDH1A1 (Figure 8a). Western blot analysis confirmed this result as well. Besides, HY1-Pt also showed a dose-dependent inhibition effect on ALDH1A1 in A549/cDDP^{CD44}^{bright} cells (Figure 8b). SOX2, OCT4, and Nanog, essential transcription factors to maintain the characteristics of stem cells, are currently recognized as the signature genes of CSCs, which have an important effect in maintaining self-renewal, proliferation, and pluripotency in malignant tumors.⁵³ To evaluate the impact of HY1-Pt on cancer cell stemness, we quantitatively analyzed the transcription levels of the signature genes of CSCs in A549/cDDP^{CD44}^{bright} cells. As illustrated in Figure 8c, the transcript levels of the transcription factors in A549/cDDP^{CD44}^{bright} cells treated with cisplatin and HY1-Pt were significantly different. The transcript levels of Nanog were obviously increased after being treated with cisplatin, showing its anti-differentiation effect on CSCs, which would lead to the enrichment of the CSC population, in accordance with earlier reports.⁵¹ Importantly, Nanog was down-regulated after being treated with HY1-Pt, indicating a diversion of the population from stemness. Due to the synergistic effect of Nanog with SOX-2

and OCT4, there is no doubt that HY1-Pt significantly down-regulated the expression of SOX-2 and OCT4 as well, whereas cisplatin showed the opposite effect. This has a correlation with the capability of HY1-Pt to influence stem cells, but cisplatin preferentially attacks non-stem cells, promoting the CSC level in the cell population. In addition, the multicellular sphere formation of A549/cDDP^{CD44}^{bright} cells after treatment with cisplatin and HY1-Pt at different concentrations, respectively, was evaluated. Obvious phenotypic changes happened in these A549/cDDP^{CD44}^{bright}-derived tumorsphere in each group. Compared with the control group, the size and number of A549/cDDP^{CD44}^{bright}-derived tumorsphere treated with HY1-Pt were significantly reduced, the larger the drug concentration is, the smaller the volume and the less the number of tumorsphere are. Although cisplatin has no significant effect on the number and size of tumorsphere, it may promote the growth of tumorsphere when the concentration is high (Figure 8d,e). These results hint that our Pt(II)-based compound may overcome cisplatin resistance by inhibiting cancer cell stemness.

It is known that stem cells are primarily controlled by Wnt/β-catenin, Notch, Hedgehog/Gli1, and BMI-1 signal transduction pathway.⁵⁴ Therefore, we tried to learn how HY1-Pt affects Wnt/β-catenin CSCs signal transduction pathway in A549/cDDP cells via western blot technique. As illustrated in Figure 8f, the expression of anticancer protein DKK1 was upregulated with the increasing concentrations of HY1-Pt, while that of the phosphorylation of GSK-3β^(ser9) protein was significantly down-regulated. In addition, HY1-Pt significantly inhibited β-catenin in a dose-dependent manner in A549/cDDP cells. Therefore, HY1-Pt can inhibit the signaling pathway of Wnt/β-catenin. It has already been proved that in

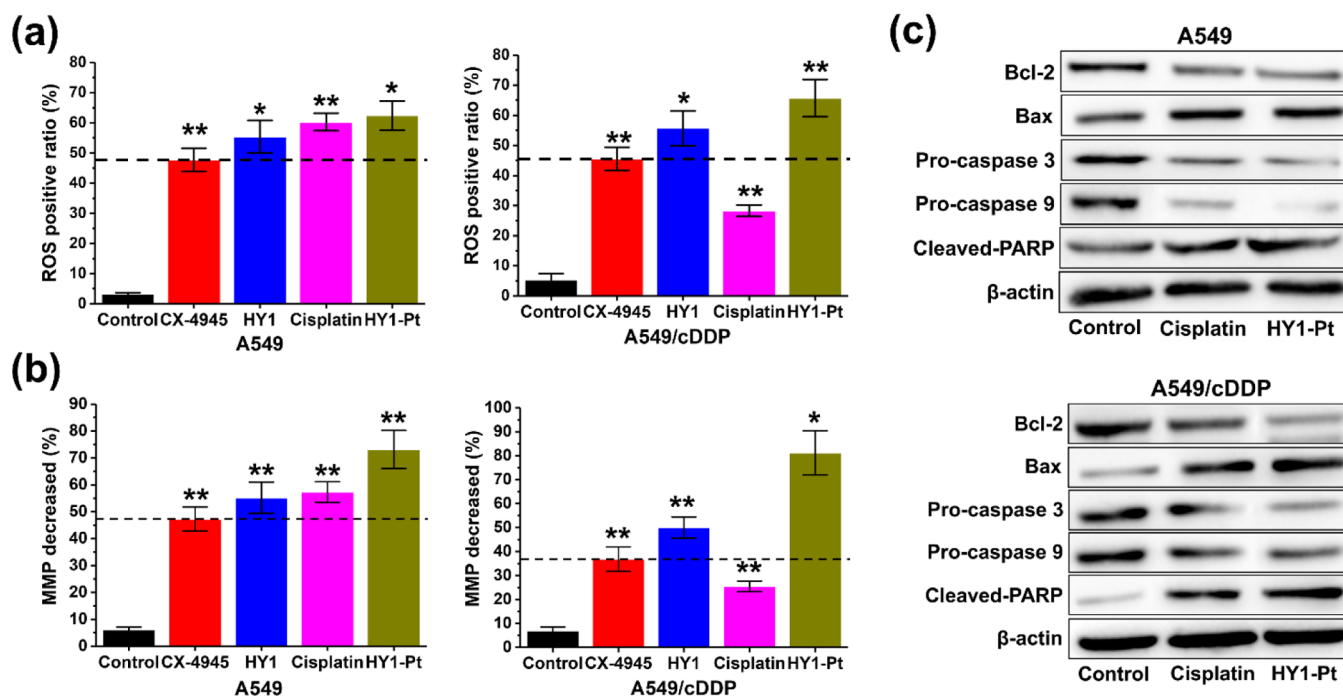


Figure 9. Study on mitochondrial apoptosis pathway. Statistical changes of (a) ROS-positive cells and (b) MMP in A549 and A549/cDDP cell treatment with CX-4945, HY1, cisplatin, and HY1-Pt at 20 μ M for 24 h. (c) Expression levels of Bcl-2, Bax, pro-caspase 3, pro-caspase 9, and cleaved-PARP in A549 and A549/cDDP cells were explored via western blot after treatment with cisplatin and HY1-Pt at 20 μ M for 24 h. Error bars = SD ($n = 3$), * $P < 0.05$, ** $P < 0.01$.

the nucleus, β -catenin binds to TCF/LEF transcription factor family to activate the promoter of target genes of β -catenin, thus activating the target genes of Wnt signaling pathway like CD44, CD24, CD133, ABCG2, ALDH1A1, EpCAM, MMP7, Vimentin, and Slug. As Wnt1 can increase expression of ALDH1A1, it promotes the expression of Akt and β -catenin as well.⁵⁵ Phosphorylated Akt has been reported to inactivate GSK-3 β by the phosphorylation of GSK-3 β at ser9, suppressing its capability to degrade β -catenin.^{56,57} So, it is suggested that HY1-Pt might regulate the expression of ALDH1A1 and CD133 via the Akt-GSK-3 β (ser9)-Wnt/ β -catenin signaling pathway, thereby inhibiting cancer cell stemness.

2.9. Study on Mitochondrial Apoptosis Pathways.

Reactive oxygen species (ROS) are inevitable products of cell metabolism, but accumulation of ROS usually oxidizes and damages the mitochondria of cells, and metal compounds induce excess ROS accumulation by disrupting intracellular redox equilibrium.⁵⁸ Mitochondria has emerged as a crucial coordinator of the cell death signaling network, including stimulation of caspases and other processes related to cell death.⁵⁹ The mitochondrial membrane potential (MMP) change in cancer cells is also considered as a key pro-apoptotic marker for early apoptosis.⁶⁰ Therefore, it is interesting to investigate whether HY1-Pt can induce production of intracellular ROS, thereby reducing MMP and then inhibiting the caspase signaling pathway. As shown in Figures 9a and S8, in A549 and A549/cDDP cells, HY1-Pt can induce the production of a large amount of intracellular ROS, and the proportion of ROS-positive cells is 62.4 and 65.7%, respectively. In contrast, in A549/cDDP cells, the amount of ROS induced by cisplatin is significantly lower than that of HY1-Pt, the proportion of ROS-positive cells induced by cisplatin is 2.32-times lower than that of HY1-Pt. Images of

ROS in two cancer cells stained with DCFH-DA (Figure S9) also indicate that the fluorescence intensity of HY1-Pt is greater than that of cisplatin, confirming the result obtained by flow cytometry. In order to investigate the ROS damage to the mitochondrial membrane by HY1-Pt, we measured the change of MMP by fluorescent probe JC-1. As shown in Figures 9b and S10, in both A549 and A549/cDDP cells, HY1-Pt can seriously induce JC-1 monomer, especially in A549/cDDP cells, the number of JC-1 monomers induced by HY1-Pt is 3.19-fold as much as that by cisplatin. Meanwhile, more JC-1 monomers were observed in cells treated with HY1-Pt in fluorescent images (Figure S11). As illustrated in Figure 9c, HY1-Pt can significantly inhibit the caspase signaling pathway, which is manifested as the decreased expression of pro-caspase-3 and pro-caspase-9 compared to the control group. Moreover, significant up-regulation of Bax, cleaved-PARP, and down-regulation of Bcl-2 in A549/cDDP cells were observed after treatment of HY1-Pt, which were greater than those induced by cisplatin. Different from the dysfunction of cisplatin in A549/cDDP cells owing to drug resistance, HY1-Pt behaved in the same way as that in A549 cells as well. These results imply that as a potent Pt(II) antitumor agent, HY1-Pt can induce to produce a great deal of ROS, reduce MMP, and promote the apoptosis of cancer cells through the mitochondrial apoptosis pathway.

2.10. Pharmacokinetic Study. As the main hydrolytic product of HY1-Pt, HY1 generated by the hydrazine bond-breaking under a tumor acidic condition was first studied in human, rat, and mouse liver microsomes for evaluating its metabolic stability. As shown in Table 2, the metabolism of HY1 is not much stable in these three types of liver microsomes. In addition, the clearance rate (Cl_{int}) of HY1 in these liver microsomes is rather fast, especially in the mouse liver ones.

Table 2. Liver Microsomal Enzyme Stability of HY1

HY1	species		
	human	rat	mouse
$T_{1/2}^a$ (min)	23.88	37.83	15.55
Cl_{int}^b (mL/min/kg)	72.80	65.66	351.00

^a $T_{1/2}$ is defined as half-life. ^b Cl_{int} is defined as clearance.

In addition, the pharmacokinetic (PK) analysis of **HY1-Pt** in Sprague-Dawley (SD) rats following a single 10 mg/kg dose administration by intravenous injection (iv) was performed. As summarized in Table 3, **HY1-Pt** demonstrated a moderate

Table 3. Pharmacokinetic Parameters of HY1-Pt and Cisplatin in SD Rats

parameter	dose (10 mg/kg)	
	HY1-Pt	cisplatin ^a
$T_{1/2}/h$	5.1 ± 0.6	5.9 ± 0.7
$CL/L\cdot h^{-1}\cdot kg^{-1}$	3.9 ± 0.5	0.06 ± 0.0
$AUC_{0-t}/ng\ h\cdot mL^{-1}$	2857 ± 374.0	26920 ± 2050
$AUC_{0-\infty}/ng\ h\cdot mL^{-1}$	2611 ± 371.0	66370 ± 6360
$V_d/L\cdot kg^{-1}$	28.9 ± 7.0	0.6 ± 0.1
MRT_{0-t}/h	2.7 ± 0.0	
$MRT_{0-\infty}/h$	2.7 ± 0.01	7.0 ± 0.8

^aData were adopted from ref 61.

half-life and plasma clearance. In addition, **HY1-Pt** also had a good apparent volume of distribution, a relatively larger area under the concentration–time curve, and an acceptable mean residue time. We also compared the pharmacokinetics of **HY1-**

Pt with that of cisplatin reported by Tanji Takada and co-workers.⁶¹ At the same dosage (10 mg/kg) by the same administration (iv), the half-life ($t_{1/2}$) of cisplatin in rats is 5.94 h, slightly higher than that of **HY1-Pt** (5.1 h). However, cisplatin was found to be difficultly eliminated with a clearance rate (CL) of 0.06 L·h⁻¹·kg⁻¹, and the residence time is long (MRT = 7.0 h). In comparison, **HY1-Pt** has a higher clearance rate (CL = 3.9 L·h⁻¹·kg⁻¹) and shorter mean residence time (MRT = 2.7 h) in rats. These data indicated that **HY1-Pt** had an acceptable PK behavior superior to cisplatin, which encouraged us to conduct *in vivo* tests on its anti-tumor activity.

2.11. In Vivo Antitumor Activity. Based on the above study, *in vivo* antitumor tests of **HY1-Pt** in A549 xenograft models were undertaken, in which animals were randomly divided into five groups as vehicle, cisplatin (4 mg/kg), and **HY1-Pt** at three doses (10, 20, 40 mg/kg). Due to the severe toxicity of cisplatin, its dose was limited only to the equal molar amount of platinum in **HY1-Pt** dosed at 10 mg/kg. As illustrated in Figure 10, the inhibitory rate (86.92%) of **HY1-Pt** at low dose (10 mg/kg) is even higher than that (66.51%) of cisplatin (4 mg/kg), despite two agents exhibited comparable *in vitro* cytotoxicity against A549 cells. It is noticed that **HY1-Pt** displayed a dose-dependent inhibitory effect on tumor growth with a maximum inhibitory rate of 95.03% at 40 mg/kg.

To learn whether **HY1-Pt** can overcome cisplatin resistance *in vivo*, we also tested the antitumor activity of **HY1-Pt** at two doses (10 and 20 mg/kg) in A549/cDDP xenograft mice with cisplatin as the positive drug. The mice were administered with the formulations in the same way as that in the A549 xenograft

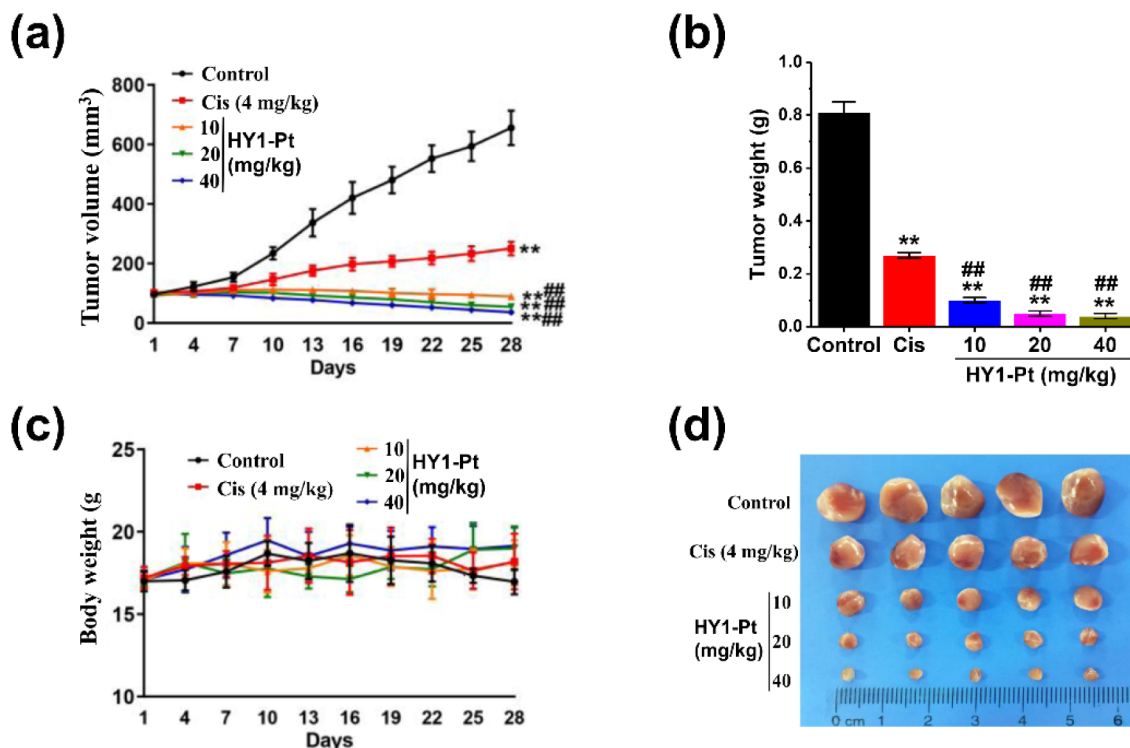


Figure 10. *In vivo* A549 xenograft model study of **HY1-Pt** and cisplatin. (a) During the observation period, tumor volumes of animals from each group, including vehicle, cisplatin (4 mg/kg, iv, once a week for 4 weeks) and **HY1-Pt** (10, 20 and 40 mg/kg, iv, once a week for 4 weeks). (b) Weights of tumors resected from all groups of mice on the last day. (c) Influence of different samples on body weight changes of the animals. (d) Images of tumors from five groups of mice at the end of the experiment. Error bars = SD ($n = 5$), ** $P < 0.01$, ## $P < 0.01$.

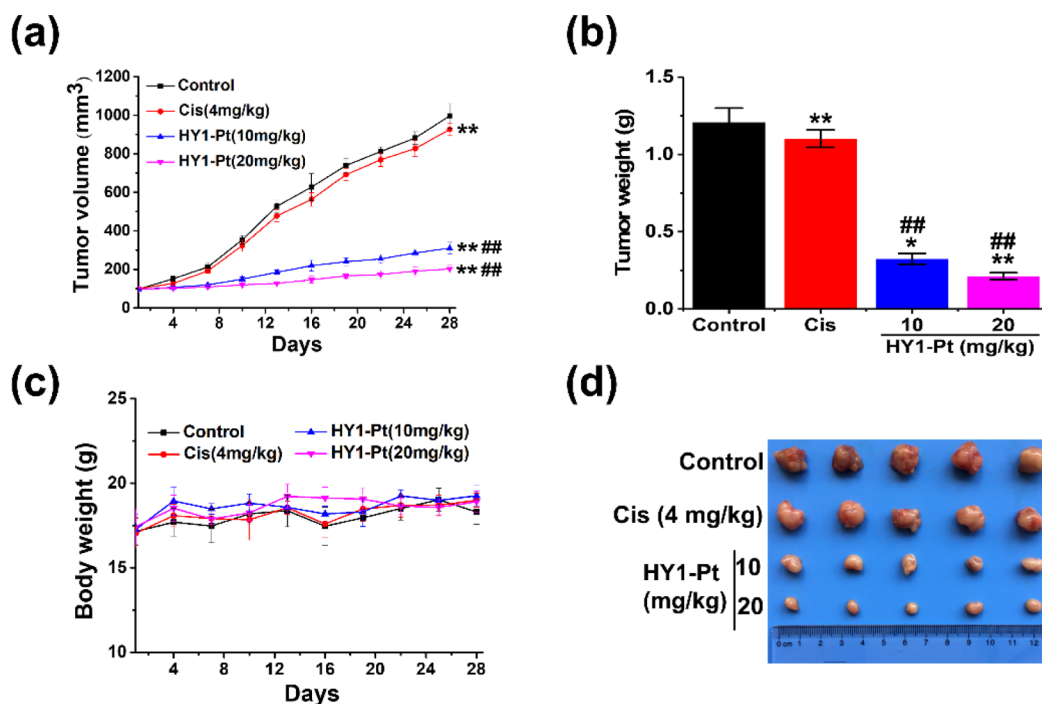


Figure 11. *In vivo* A549/cDDP xenograft model study of HY1-Pt and cisplatin. (a) During the observation period, tumor volumes of animals in each group, including vehicle, cisplatin (4 mg/kg, iv, once a week for 4 weeks), and HY1-Pt (10 and 20 mg/kg, iv, once a week for 4 weeks). (b) Weights of tumors resected from all groups of sacrificed mice on the last day. (c) Influence of different samples on body weight changes of the animals. (d) Images of tumors from five groups of mice at the end of the experiment. Error bars = SD ($n = 5$), ** $P < 0.01$, ## $p < 0.01$.

model. As shown in Figure 11, cisplatin dosed at 4 mg/kg displays much weaker activity with an inhibitory rate of 9.09% owing to the serious resistance as predicted. However, HY1-Pt dosed at 10 mg/kg with an equivalent molar amount of platinum in cisplatin is able to effectively inhibit the tumor growth at a rate of 72.72%. Particularly, HY1-Pt dosed at 20 mg/kg has the highest inhibitory rate of 82.64%, showing the dose dependence of HY1-Pt treatments.

More significantly, there is no conspicuous change in body weight in all the mice treated with HY1-Pt, revealing that HY1-Pt has low systemic toxicity and good safety (Figures 10c and 11c). Furthermore, the H.E. staining of slices from heart, liver, spleen, lung, and kidney of an animal randomly selected from each tested group in both A549 and A549/cDDP models demonstrates that HY1-Pt at the used dosages has almost no toxic effects on organ tissues compared with cisplatin (Figures S12 and S13). These results indicate that HY1-Pt not only effectively inhibits cisplatin-mediated resistance in NSCLC cells *in vitro* but also exhibits strong anticancer activity with low toxicity both in the A549 xenograft model or in the A549/cDDP xenograft models.

3. CONCLUSIONS

Our study indicates that HY1-Pt has potent cytotoxicity activity toward the cancer cells of the tested but with low toxicity in normal cells. Notably, cisplatin-induced resistant cancer cells are also sensitive to HY1-Pt as expected. Further research on the mechanism of action reveals that HY1-Pt can target CK2 protein, reinforce cellular accumulation of platinum, inhibit cancer cell stemness, and suppress DNA damage repair, effectively reversing cisplatin resistance through the signaling pathway of Wnt/ β -catenin by inhibiting expression of the signature genes of CSCs in A549/cDDP cancer cells and CK2 overexpression. Besides, treatment of

cancer cells with HY1-Pt can dramatically increase the level of ROS, reduce MMP, and promote apoptosis of cancer cells through the mitochondrial apoptosis pathway. More significantly, HY1-Pt can effectively overcome cisplatin resistance, exhibiting potent *in vivo* antitumor activity in both A549 and A549/cDDP xenograft models with low toxicity. Overall, as the first example of a CSC inhibitor used in conjugation with other bioactive species in a molecular entity for drug resistance reversal, HY1-Pt has a potential as a Pt(II)-based drug to treat with all kinds of solid tumors including NSCLC.

4. EXPERIMENTAL SECTION

4.1. Materials and Instrument. All chemicals in analytical purity were purchased commercially from InnoChem (Beijing) Technology Co., Ltd. and Sann Chemical Technology (Shanghai) Co., Ltd. and used without further purification. DN604 and BBI608 were synthesized according to the method reported in previous literature.^{38,62} ¹H and ¹³C NMR spectra were recorded on a Bruker 600 MHz spectrometer. High-resolution mass spectroscopy (HR-MS) was measured by an Agilent 6224 ESI/TOF MS instrument. The purity of the compounds was detected by a reversed-phase high performance liquid chromatogram (RP-HPLC) (waters, 2545 system) on an ODS column (250 × 4.6 mm, 5 μ m). Flow cytometry studies were performed on a BD FACSCalibur flow cytometer. An Olympus FV1000 confocal microscope was used to record the confocal images. Besides, all cells used in this work were purchased from Biorn Lifescience Co., Ltd. Pro-caspase 3, Pro-caspase 9, Bcl-2, Bax, Cleaved-PARP, phosphor-AKT (ser129), phosphor-Cdc37 (ser13), ALDH1A1, γ -H2AX, MDC1, DKK1, phospho-GSK-3 β (ser9), β -catenin, and β -actin antibodies were all purchased from Beyotime Biotechnology.

4.2. Chemistry. **4.2.1. Synthesis and Characterization of Compound 7 and CX-4945.** Compound 7 and CX-4945 were synthesized in accordance with the procedures reported previously.²⁵ Compound 7: ¹H NMR (600 MHz, DMSO-*d*₆): δ 10.09 (s, 1H), 9.91 (s, 1H), 8.94 (d, $J = 5.6$ Hz, 1H), 8.79 (d, $J = 8.5$ Hz, 1H), 8.77 (d, $J =$

5.6 Hz, 1H), 8.34 (t, $J = 1.9$ Hz, 1H), 8.17 (dd, $J = 6.3, 1.4$ Hz, 1H), 7.90 (dd, $J = 8.4, 1.7$ Hz, 1H), 7.42 (t, $J = 8.1$ Hz, 1H), 7.12 (dd, $J = 7.9, 1.4$ Hz, 1H), 3.92 (s, 1H) ppm. **CX-4945**: ^1H NMR (600 MHz, DMSO- d_6): δ 12.04 (s, 1H), 10.30 (s, 1H), 10.16 (s, 1H), 9.08 (d, $J = 5.8$ Hz, 1H), 9.00–8.97 (m, 1H), 8.94 (d, $J = 8.5$ Hz, 1H), 8.31–8.28 (m, 2H), 8.12 (d, $J = 8.2$ Hz, 1H), 8.03 (dd, $J = 8.4, 1.5$ Hz, 1H), 7.45 (t, $J = 8.1$ Hz, 1H), 7.17 (d, $J = 7.9$ Hz, 1H) ppm.

4.2.2. Synthesis and Characterization of HY1. To a solution of compound **7** (1.09 g, 3 mmol) in MeOH (20 mL) was slowly added hydrazine hydrate (1.5 g, 30 mmol) at room temperature. The reaction mixture was heated to reflux for 72 h and monitored with thin layer chromatography (TLC). After the substrate was completely consumed, the reaction liquid was slowly poured into the ice water mixture to separate out the yellow solid, filtering the precipitate, and washed with ice methanol (3×10 mL) to obtain the crude product of **HY1**. The crude product was recrystallized with 1, 4-dioxane (10 mL) to get a bright yellow solid (0.989 g). Yield: 90.8%. ^1H NMR (600 MHz, DMSO- d_6): δ 10.14 (s, 1H), 10.08 (s, 1H), 9.63 (s, 1H), 8.95 (d, $J = 6.0$ Hz, 1H), 8.80 (d, $J = 12.0$ Hz, 1H), 8.55 (d, $J = 6.0$ Hz, 1H), 8.33 (t, $J = 1.8$ Hz, 1H), 8.21 (d, $J = 1.6$ Hz, 1H), 8.07 (d, $J = 6.0$ Hz, 1H), 7.91 (dd, $J = 12.0, 1.6$ Hz, 1H), 7.42 (t, $J = 6.0$ Hz, 1H), 7.12 (dd, $J = 8.0, 1.4$ Hz, 1H), 4.63 (s, 2H) ppm. ^{13}C NMR (150 MHz, DMSO- d_6): δ 165.77, 150.47, 148.13, 147.69, 143.76, 142.40, 134.73, 133.35, 130.52, 127.52, 126.26, 124.17, 123.00, 122.83, 122.60, 121.47, 120.57, 119.56, 116.79 ppm. HR-MS (m/z): (ESI) calcd for $\text{C}_{19}\text{H}_{14}\text{ClN}_5\text{O}$ [$\text{M} + \text{H}$] $^+$, 364.0965; found, 364.0967.

4.2.3. Synthesis and Characterization of HY1-Pt. **HY1** (0.181 g, 0.5 mmol), **DN604** (0.193 g, 0.5 mmol), and 3–5 drops of acetic acid were mixed in methanol (20 mL). The mixture was stirred and heated at 60 °C for 48–72 h in the dark. The reaction was monitored by TLC. After the reaction finished, the resulting deposits were filtered and washed with methanol (3×10 mL) to obtain the crude product **HY1-Pt**. The crude product was recrystallized with dimethylformamide (DMF)/1, 4-dioxane (1:4, v/v) to get a bright yellow solid (0.365 g). Yield: 93.4%. ^1H NMR (600 MHz, DMSO- d_6): δ 11.15 (s, 1H), 10.19 (s, 1H), 9.67 (s, 1H), 8.99 (d, $J = 4.2$ Hz, 1H), 8.86 (d, $J = 7.7$ Hz, 1H), 8.58 (d, $J = 3.8$ Hz, 1H), 8.26 (s, 1H), 8.23 (s, 1H), 8.14 (d, $J = 7.2$ Hz, 1H), 7.93 (d, $J = 7.3$ Hz, 1H), 7.45 (t, $J = 7.5$ Hz, 1H), 7.14 (d, $J = 6.9$ Hz, 1H), 4.26 (s, 6H), 3.74 (s, 4H) ppm. ^{13}C NMR (150 MHz, DMSO- d_6): δ 176.45, 176.23, 163.28, 159.72, 150.55, 148.18, 147.80, 143.63, 142.33, 135.12, 133.28, 130.62, 127.50, 126.91, 124.23, 123.84, 122.80, 122.69, 121.73, 120.64, 119.68, 116.83, 56.40, 49.60, 46.96 ppm. HR-MS (m/z): (ESI) calcd for $\text{C}_{25}\text{H}_{22}\text{ClN}_7\text{O}_5\text{Pt}$ [$\text{M} + \text{H}$] $^+$, 731.1091; found, 731.1353.

4.3. Purity of Final Compounds. The purity of all final compounds was determined by RP-HPLC (waters e2695, US) equipped with an ODS column (250×4.6 mm, 5 μm) and a 2489 UV/vis detector. Detailed steps: **CX-4945**, **HY1**, and **BB1608** were dissolved in chromatographic pure methanol and filtered by organic syringe filters of 0.45 μm aperture. The purity of these compounds was investigated at 25 °C as the column temperature, using acetonitrile/water (55:45, v/v) as the mobile phase at the flow rate of 0.8 mL/min. The purity of **CX-4945**, **HY1**, and **BB1608** was 99.43, 95.58, and 99.70%, respectively, analyzed by the peak area percentage method. **HY1-Pt** was dissolved with a small amount of dimethyl sulfoxide (DMSO), diluted with methanol, and filtered with an organic syringe filter of 0.45 μm aperture. The purity of **HY1-Pt** was investigated at 25 °C as the column temperature, using methanol/water (60:40, v/v) as the mobile phase at the flow rate of 1.0 mL/min. The purity of **HY1-Pt** was 97.40%, analyzed by the peak area percentage method.

4.4. CK2 Activity Assay. CK2 kinase (human) assay/inhibitor screening assay kit and CK2 enzyme were purchased from Shanghai Fusheng Industrial Co., Ltd. (Shanghai, China). The inhibitory activity of **CX-4945**, **HY1**, and **HY1-Pt** on CK2 enzyme was detected according to manufacturer's instruction provided in the CK2 assay kit. Briefly, the CK2 reaction solution was added into each well of 96-well plates after thawing, and five different concentrations of **HY1-Pt** (500.00, 100.00, 20.00, 1.00, 0.80 nM) were added to each well as the "test inhibitor" and five different concentrations of **CX-4945** and **HY1**

(500.00, 100.00, 20.00, 1.00, 0.80 nM) were added to the well as the "positive control", with the same solution without the inhibitor as "blank". After sealing the plate with a sealing film, the setup was incubated at 37 °C for 30 min. After that, conjugate reagent (50 μL) was added to each well, excepting blank holes, and incubated at 37 °C for another 30 min. The color developing reagents A (50 μL) and B (50 μL) were successively added to each hole, and the mixture was shaken gently and mixed well, avoiding light for 10 min, and then stop buffer (50 μL) was added to each hole. The reaction mixtures were incubated at room temperature for 10 min and the value of O.D. was measured via an enzyme-labeling instrument at a wavelength of 490 nm. The IC_{50} value of each compound represented as the mean \pm SD was obtained by three parallel experiments.

4.5. Western Blot Tests. A549 and A549/cDDP cells were diluted into 1×10^5 cells/mL mixed liquid with the corresponding medium and spread in a six-well plate and cultured at 37 °C for 12 h and then treated with 20 μM of the tested compounds for 24 h. Two cancer cells were collected, centrifuged, and washed with phosphate buffer saline (PBS) and then lysed in lysis buffer (100 mM Tris-Cl, pH 6.8, 4% (m/v) sodium dodecyl sulfonate, 20% (v/v) glycerol, 200 mM β -mercaptoethanol, 1 mM phenylmethylsulfonyl fluoride, and 1 g/mL aprotinin) and centrifuged at 15000 rpm for 15 min at 4 °C and collected. The concentrations of total proteins were measured with BCA protein assay reagents (Imgenex, USA). Protein (20–100 μg) prepared from the indicated cells was loaded per lane and electrophoresed in 8 or 10% sodium dodecyl sulfate polyacrylamide gel electrophoresis and then transferred to poly(vinylidene difluoride) Hybond-P membrane (GE Healthcare) using a transblot apparatus (Bio-Rad, USA). The blots were blocked with 5% nonfat milk in Trisbuffered saline with Tween 20 (TBST) buffer for 1 h and co-incubated with primary antibodies (anti-p-AKT(ser129), anti-p-Cdc37(ser13), anti-ALDH1A1, anti- γ -H2AX, anti-DKK1, anti-p-GSK3 β (ser9), anti- β -catenin, anti-Bcl-2, anti-Bax, anti-pro-caspase-3, anti-pro-caspase-9, anti-cleaved-PARP, and anti- β -actin) and diluted in TBST overnight at 4 °C. The membrane was washed with TBST and incubated with secondary antibodies conjugated with peroxidase for 2 h at 37 °C, then washed twice with TBST buffer and PBS once, and visualized with chemiluminescence reagent (Thermo Fischer Scientific Ltd.).

4.6. ALDH1A1 Enzyme Activity Assay. ALDH1A1 kinase (human) assay/inhibitor screening assay kit and ALDH1A1 enzyme were purchased from Shanghai Fusheng Industrial Co., Ltd. (Shanghai, China). The inhibitory activity of **CX-4945** and **HY1** on ALDH1A1 enzyme was detected according to manufacturer's instruction provided in the ALDH1A1 assay kit. The specific test procedure is the same as the CK2 kinase (human) assay/inhibitor screening assay kit.

4.7. Cell Culture. Six different cells were used in this experiment including A549 (non-small cell lung cancer), A549/cDDP (cisplatin-resistant lung cancer), PC-3 (prostate cancer), HepG2 (liver cancer), T24 (bladder cancer), and LO2 (normal live cells). All of them were originally purchased from the Cell Bank of Shanghai Institute of Cell Biology. A549, A549/cDDP, and PC-3 cells were cultured with a complete medium containing 10% fetal bovine serum (FBS) and 90% Roswell Park Memorial Institute-1640 (RPMI-1640) incomplete medium at 37 °C in 5% CO_2 . HepG-2, T24, and LO2 cells were cultured at 37 °C in 5% CO_2 with Dulbecco's modified Eagle medium supplemented with 10% FBS. The culture medium was also supplemented with D-glucose of 2 g/L, L-glutamine of 0.3 g/L, sodium bicarbonate of 2 g/L, penicillin of 80 U/mL, and streptomycin of 0.08 mg/mL, kept in a constant temperature incubator containing 5% CO_2 at 37 °C.

4.8. Detection of ALDH Activity. For the evaluation of the expression levels of ALDH1A1 in A549 cells exposed to **CX-4945** (20 μM) and **HY1** (20 μM), ALDEFLUOR (Stem cell Technologies, Vancouver BC, CA) staining was measured using the FITC channel of fluorescent activated cell sorting according to the manufacturer's instruction.

4.9. Real-Time Quantitative PCR. Total RNA was isolated by using TRIZOL from A549 and A549/cDDP^{CD44^{bright}} cells treated for

24 h with equitoxic concentration of tested compounds corresponding to $IC_{50/72h}$. RNA was reverse-transcribed with Luna universal one-step RT-qPCR (GeneAmp 9600, PerkinElmer), and the resulting cDNA was subsequently submitted to thermal cycling on Quantitative Real-time PCR (ABI step one plus, ABI). The thermal profile was as follows: reverse transcription for 10 min at 55 °C, initial denaturation for 1 min at 95 °C, followed by 39 thermal cycles of denaturation for 10 s at 95 °C, and extension for 30 s at 60 °C. Primer sequences are listed in Table S2. All runs included melting curve analysis and template-free negative technical controls to confirm specific single-product amplification. β -actin mRNA was used as an internal control. The relative expression of mRNA is represented as fold increase ($2^{-\Delta\Delta Ct}$).⁶³

4.10. Spheroid Formation Assay. Briefly, the A549 and A549/cDDP^{CD44^{bright}} cells were plated on Ultra-Low Attachment Surface 24 well-plates (3473, Corning) in serum-free 1640 medium supplemented with B27 (1:50, 17504044, Invitrogen), epidermal growth factor (EGF) (20 ng/mL, AF-100-15, Peprotech), and β -fibroblast growth factor (β -FGF) (10 ng/mL, 100-18B, Peprotech) at a density of 800 cells per well. When the number of cells in a spheroid were more than 10, it was considered to have formed a clone sphere. After treatment with different drug formulations for 10 days. The number and sizes of tumorsphere were measured on day 10.

4.11. Assessment of CD44 Expression. A549 cells were seeded on 6-well plates at the density of 1×10^5 cells per well. After incubating the samples for 12 h, the cells were treated with CX-4945 (20 μ M), BBI608 (20 μ M), and HY1 (20 μ M), respectively, for 24 h. Then, the cells were stained with FITC-conjugated anti-CD44 according to the manufacturer's respective instructions. CD44 expressions were assessed by flow cytometry. Calculation of inhibition rate was based on fluorescence intensity.

4.12. Stability of HY1-Pt. HY1-Pt was dissolved in pH = 6.0 and 7.4 Hepes buffer (0.25 M) containing 2% DMF and incubated at 37 °C in the dark, respectively. The solution behavior of HY1-Pt was detected and recorded by UV-vis (Shimadzu UV-2600) with wavelength ranging from 225 to 450 nm and scanned every 30 min for a total of 24 times. In addition, the stability of HY1-Pt was also detected by RP-HPLC (waters, 2545 system) on an ODS column (250 \times 4.6 mm, 5 mm) at different time points with an eluent of methanol/water (60:40, v/v) at a flow rate of 1 mL/min.

4.13. Measurement of Water/Octanol Partition Coefficient ($\log P_{O/W}$). The lipophilicity ($\log P_{O/W}$) of HY1-Pt was measured using the shake-flask method in the 1-octanol/distilled water system. Octanol was saturated with a distilled water by shaking the two-phase mixture overnight. A portion of 5 mL of pre-saturated octanol containing HY1-Pt was incubated with 5 mL of distilled water in a 15 mL tube. The tube was shaken at room temperature in the dark for 24 h. Centrifugation was carried out at 2500 rpm for 15 min to separate different phases, and the platinum concentrations in these two phases were determined by ICP-MS. The final result was expressed as a mean of three independent experiments. The $\log P_{O/W}$ was calculated using the following equation

$$\log P_{O/W} = \log\left(\frac{[C]_{\text{initial}} - [C]_{\text{final}}}{[C]_{\text{final}}}\right)$$

4.14. Cytotoxicity Measurement. MTT assay was used to evaluate the cytotoxicity of all compounds synthesized in this work. Different cells were grown on 96-well plates at a cell density of 1×10^5 cells/mL and incubated at an atmosphere of 5% CO₂ and 95% air at 37 °C for 12 h. After the cells were completely attached, the complete medium was replaced, and the samples were diluted into five concentrations and added to the wells in turn. Each concentration was set up with three identical experimental groups to ensure that the volume of each well was 100 μ L. The MTT (3-(4,5)-dimethylthiazoliazolo(-z-yl)-3,5-di-phenyltetrazoliumromide) solution with the concentration of 5 mg/mL was added to each well after 72 h. Next, the culture medium was removed and about 100 μ L of DMSO was added to each well to dissolve completely after 3–4 h. The O.D. value was read at 490 nm enzyme labeling instrument. The IC_{50} values of each group can be calculated by SPSS software.

4.15. Cell Cycle Test. A549 and A549/cDDP cells were diluted into 1×10^5 cells/mL mixed liquid with the corresponding medium and spread in a six-well plate and cultured at 37 °C for 12 h. Two cancer cells were incubated with 20 μ M of the tested compounds for 24 h. The cells were collected into different centrifugal tubes, added about 500 μ L of 70% ice ethanol, and placed at -20 °C for overnight. Centrifugation was carried out at 1500 rpm for 5 min to remove the supernatant, and then 1 mg/mL PI staining solution (containing 10% RnaseA) was added to the cells and stored in the dark for 30 min. The sample was measured via flow cytometry (FAC Scan, Becton Dickinson), and the data was analyzed with FlowJo software (TreeStar, Inc.).

4.16. Apoptosis Assessment. Detection of apoptosis of A549 and A549/cDDP induced by CX-4945, HY1, cisplatin, and HY1-Pt was made by the Annexin V-FITC apoptosis detection kit according to the manufacturer's protocol. The A549 and A549/cDDP cells in logarithmic growth phase were collected and suspended with the corresponding culture medium after centrifugation and plated on a six-well plate with a cell concentration of 1×10^5 cells per well. After the cells have completely adhered to the wall, the original culture medium was replaced with a fresh medium and treated with 20 μ M of the tested compounds, respectively, for 24 h at 37 °C. Then, the cells were incubated with Annexin V-FITC and then PI for 10 min in the dark at room temperature; cells were analyzed by flow cytometry (FAC Scan, Becton Dickinson) and the apoptosis value was obtained using Cell-Quest software (BD Biosciences).

4.17. Cellular Accumulation of Platinum. A549 and A549/cDDP cells with a concentration of 1×10^5 cells/mL were seeded in 6-well plates until reached about 80% confluence and then incubated with cisplatin (20 μ M) and HY1-Pt (20 μ M), respectively, at 37 °C. The cells were harvested and stored in a different centrifuge after 12 h co-incubation, washed with cold PBS (3 \times 3 mL), and digested with 200 mL 65% HNO₃ to obtain a completely uniform solution. After diluted with pure water, intracellular platinum content was detected via ICP-MS.

4.18. Comet Assay. A549 and A549/cDDP cells were incubated with 20 μ M of the tested compounds for 12 h, combined with molten LM Agarose (Trevigen) at a ratio of 1:10 (v/v), and pipetted onto Comet Slide (Trevigen) immediately. In the dark, slides were incubated at 4 °C for 10 min, and then the cells were immersed in prechilled Lysis buffer and incubated at 4 °C for 60 min. In the dark, the DNA was immersed in the alkaline solution of pH > 13 (200 mM NaOH, 1 mM EDTA) for 40 min. Single cell electrophoresis was carried out at 25 V voltage for 25 min via alkaline electrophoresis solution (200 mM NaOH, 1 mM EDTA). The slides were rinsed with Tris-HCl solution of 0.4 mM of pH = 7.5 three times, stained with PI for 30 min in the dark, and visualized by microscopy.

4.19. Immunofluorescence Test. Briefly, A549 and A549/cDDP cells were grown to confluence in sterile watchglasses for 24 h at 37 °C and then treated with 20 μ M of CX-4945, HY1, cisplatin, and HY1-Pt for 24 h. All cells were washed with PBS, fixed in 4% paraformaldehyde/PBS for 30 min, and permeabilized with PT-5 solution [0.3% Triton X-100 in PBS] for 30 min at 4 °C. The cells were blocked by incubating with PTB-5 [0.5% BSA in PBS] for 1 h at room temperature. Dishes were then incubated with the primary antibody (1:500) overnight at 4 °C. Cells were stained with the secondary antibody conjugated with Alexa 488 (1:100, Invitrogen, Carlsbad, USA). Microscopy was performed on a Leica TCS NT confocal scanner equipped with an ArKr-Laser on the Leica DM IRBE inverted microscope (lens: HCX PlanApo 63x oil/NA1.32). Confocal images were displayed as maximum projections and assembled in Adobe Photoshop 7.0.

4.20. Molecular Docking. Molecular docking of HY1-Pt to CK2 α (PDB ID: 6isj) was carried out by AutoDock, in which the Iterated Local Search Globule Optimizer was applied as optimization algorithm.⁶⁴ Ligand HY1-Pt was prepared in ChemBioDraw Ultra 14.0 and minimized with the ChemBio3D Ultra 14.0. Before the docking process, the nature ligand and water molecules were removed from the crystal structure. Subsequently, all hydrogen atoms were added to each protein and ligand to be docked, and each coordinate

file of protein and ligand was generated as PDBQT file using AutoDockTools-1.5.6. A grid box for the binding site covered the catalytic site of the protein or 50 Å in the three dimensions for the allosteric binding site. The coordinate of the binding site is $X = 33.303$, $Y = 6.104$, $Z = 14.131$. The box had 0.375 Å grid spacing and centered at the geometric center of the protein. When using Autodock software to simulate the binding mode between HY1-Pt and CK2 α protein, the force field parameters added to Pt were as follows "atom_par Pt 2.75 0.080 12.000–0.00110 0.0 0.0 0 -1 -1 1 # non H-bonding". In each docking experiment, the best binding mode was selected according to the binding affinity calculated by the scoring function in AutoDock. Docking results were analyzed and visualized with PyMOL 2.4.

4.21. A549/cDDP^{CD44}^{bright} Cell Sorting. In order to enrich the cells by CSCs, A549/cDDP cells were stained for its CSC-marker CD44 with FITC-conjugated antibodies and subsequently sorted with magnetic anti-FITC microbeads. The effectivity of sorting was further checked by flow cytometry (Figure S6a,b). CD44-birght A549/cDDP (A549/cDDP^{CD44}^{bright}) cells were selected for further experiments as CSC-like population. The A549/cDDP cells were sorted by using the magnetic separation method based on anti-fluorophore microbeads from Miltenyi Biotec, Gladbach, Germany. Briefly, A549/cDDP cells were stained with CD44-FITC for 10 min at 4 °C; then, the cells were labeled with anti-FITC microbeads for 15 min at the same temperature. Cells were magnetically sorted by using the magnetic separation method based on anti-fluorophore microbeads (MS columns).

4.22. Assessment of CD133 Expression. The A549/cDDP^{CD44}^{bright} cells were seeded on 6-well plates at the density of 1×10^5 cells per well. After incubating the samples for 12 h, the cells were treated with cisplatin (10 μ M) and different concentration of HY1-Pt, respectively, for 24 h. Then, the cells were stained with PE-conjugated anti-CD133 according to the manufacturer's respective instructions. CD133 expressions were assessed by flow cytometry. Calculation of the inhibition rate was based on fluorescence intensity.

4.23. ROS Measurement. The A549 and A549DDP cells were diluted into 1×10^5 cells/mL mixed liquid with the corresponding medium and spread in a six-well plate and cultured at 37 °C for 12 h. Two cancer cells were treated with various compounds: vehicle (DMSO), CX-4945 (20 μ M), HY1 (20 μ M), cisplatin (20 μ M), and HY1-Pt (20 μ M) for 24 h, respectively. The cells were washed two times with PBS, and 2,7-dichlorodihydrofluorescein diacetate (DCFH-DA) (Molecular Probe, Beyotime, Haimen, China) was used as a probe to measure the level of ROS according to the different fluorescence intensity by Confocal photography at the same voltage. Besides, after different groups of cells were washed twice with PBS, the production of ROS was also detected by flow cytometry.

4.24. Mitochondrial Membrane Potential Measurement. The A549 and A549DDP cells were diluted into 1×10^5 cells/mL mixed liquid with the corresponding medium and spread in a six-well plate and cultured at 37 °C for 12 h and then treated with 20 μ M of the tested compounds for 24 h. In the dark, the medium was replaced followed by staining with a JC-1 fluorescent probe for 30 min at 37 °C, and then the cells were washed twice with PBS, and the effects of various compounds on MMP of tumor cells were analyzed with flow cytometer and confocal photography.

4.25. Metabolic Stability. The metabolic stability of HY1 in incubation with human, rat, and mouse liver microsomes was determined through the commercially available service provided by Shanghai ChemPartner Co., Ltd. (Shanghai, China). Liver microsomal incubations were conducted in triplicate. Incubation mixtures (0.5 mg/mL microsome protein, pH 7.4 of 100 mM phosphate buffer, 1 μ M compounds in DMSO) were first shaken for pre-incubation at 37 °C. The reaction was initiated by adding NADPH to obtain a concentration of 1 mM NADPH in the mixture. For metabolic stability studies, aliquots of the incubation sample mixture were collected at 0, 5, 15, 30, and 45 min. After collection of samples, the reaction was terminated with DMSO containing the internal standard (200 ng/mL Tolbutamide). The mixture was then centrifuged to remove the protein, and the supernatant was subsequently applied to

S47 LC-MS/MS analysis. Positive control samples were prepared as described above, except for the test compound that was replaced with the known P450 substrate (1 μ M Midazolam).

4.26. Pharmacokinetic Assay. The pharmacokinetic profile of HY1-Pt was investigated in 12 h fasted male SD rat following a single dose given intravenous injection (iv). HY1-Pt was dissolved in DMF: Tween 80: 5% glucose injection = 10:2:88. Three male SD rats weighing about 250–270 g were treated with HY1-Pt (10 mg/kg). Blood samples (0.3 mL) of each rat were collected from the rat's posterior orbital vein at 0.0833, 0.25, 0.50, 0.75, 1, 2, 3, 4, 6, 8, 12, and 24 h following iv dosing. Samples were centrifuged at 4000 rpm for 10 min, and the plasma was collected and stored at –40 °C until analysis. Samples were analyzed by LC-MS/MS technique. The data of blood concentration (c)–time (T) measured after iv administration were processed by Das 2.0 software. The appropriate mathematical model was selected to fit, and the pharmacokinetic parameters were calculated.

Preparation of standard curves: 100 μ L of blank plasma was added to 10 μ L of the standard solution of HY1-Pt at different concentrations (30, 60, 150, 300, 600, 1500, 3000, 6000, 15000, and 30000 ng/mL), respectively, to prepare plasma samples equivalent to ropivacaine with plasma mass concentrations of 3, 6, 15, 30, 60, 150, 300, 600, 1500, and 3000 ng/mL. The samples with different concentrations (5 μ L) were analyzed by the LC-MS/MS technique, the ratio Y of the peak area of each component to the internal standard peak area was used to perform linear regression operation on the plasma mass concentration X , and the regression equation obtained was the standard curve. The regression equation of HY1-Pt is $Y = 0.6962X - 0.0137$ ($r = 0.9998$), and the minimum quantitative limit all is 3 ng/mL.

4.27. In Vivo Antitumor Efficacy of HY1-Pt. (a) A549 xenograft model: 5×10^7 A549 cells in 0.1 mL of sterile PBS were injected subcutaneously into the flank of five-week-old, weighing about 16–18 g, male BALB/c athymic nude mice; they were all purchased from Shanghai Sipo-Bikai laboratory animal co. Ltd. (China). When the tumors reached a volume of 100–120 mm³ in all mice, 25 mice were randomly divided into five groups with five mice per group and treated via intravenous injection through the tail vein with 0.1 mL 5% glucose injection (once a week for 4 weeks), cisplatin (4 mg/kg, once a week for 4 weeks), and HY1-Pt (10, 20 and 40 mg/kg, once a week for 4 weeks). Cisplatin was dissolved in normal saline, HY1-Pt was dissolved in DMF: Tween 80: 5% glucose injection = 10:2:88. Tumor volumes and body weights were recorded twice for a week. The calculation formula of tumor volume (TV, mm³) is $TV = 0.5 \times \text{length} \times \text{width}^2$. Growth curves were plotted using the average tumor volume within each experimental group at the set time points via origin 9.0. 25 mice were sacrificed after the last treatment; then tumor weight was evaluated as the antitumor activity of the corresponding groups, and the heart, liver, spleen, lung, kidney, and tumor tissues were excised for H.E. staining. The body weight and physical state of the mice were measured simultaneously as an indicator of systemic toxicity.

(b) A549/cDDP xenograft model: the procedure was the same as that of the A549 xenograft model except that A549/cDDP cells were used and HY1-Pt was given in two groups at doses of 10 and 20 mg/kg, respectively.

4.28. Statistical Analysis. The data shown in this manuscript were expressed as means \pm SD from at least three independent experiments, each in triplicate samples for individual treatment or dosage. Statistical analyses were performed using an unpaired, two-tailed Student's t -test, and significance of difference is indicated as * $P < 0.05$ and ** $P < 0.01$.

■ ASSOCIATED CONTENT

Supporting Information

The Supporting Information is available free of charge at <https://pubs.acs.org/doi/10.1021/acs.jmedchem.1c00079>.

The synthetic route of CX-4945; the proportion of CD44⁺ subsets induced by CX-4945, BBI608, and HY1;

RP-HPLC analysis on the stability of **HY1-Pt**; flow cytometry analysis on the cell cycles, apoptosis, and the expression of γ H2AX in A549 and A549/cDDP cells induced by **HY1-Pt** and related sample; the inhibitory rate curves of **HY1-Pt** on CK2 enzyme activity; flow cytometry analysis on the expression of CD133⁺ in A549/cDDP and A549/cDDP^{CD44^{bright}} cells induced by cisplatin and **HY1-Pt**; the production of ROS, changes of JC-1 and MMP in A549 and A549/cDDP cells induced by the **HY1-Pt** and related sample were detected by the flow cytometer and confocal laser scanning microscope; H.E. staining of tissues in the nude mice xenograft model of A549 and A549/cDDP; tables of the stability of **HY1** in incubation with human, rat, and mouse liver microsomes; tables of the data of the plasma concentrations at different time points after intravenous injection of **HY1-Pt** in rats; tables of the inhibitory effects of measured samples on the A549 cancer cell xenograft mice model; tables of the inhibitory effects of measured samples on the A549/cDDP cancer cell xenograft mice model; and figures of ¹H NMR, ¹³C NMR, HR-MS spectra, and RP-HPLC chromatograms (PDF)

Molecular formula strings (CSV)

Atomic coordinates of **HY1-Pt** (PDB)

AUTHOR INFORMATION

Corresponding Author

Shaohua Gou – Jiangsu Province Hi-Tech Key Laboratory for Biomedical Research and Pharmaceutical Research Center and School of Chemistry and Chemical Engineering, Southeast University, Nanjing 211189, PR China; orcid.org/0000-0003-0284-5480; Email: 2219265800@qq.com

Authors

Yuanjiang Wang – Jiangsu Province Hi-Tech Key Laboratory for Biomedical Research and Pharmaceutical Research Center and School of Chemistry and Chemical Engineering, Southeast University, Nanjing 211189, PR China

Xinyi Wang – Jiangsu Province Hi-Tech Key Laboratory for Biomedical Research and Pharmaceutical Research Center and School of Chemistry and Chemical Engineering, Southeast University, Nanjing 211189, PR China

Gang Xu – Jiangsu Province Hi-Tech Key Laboratory for Biomedical Research and Pharmaceutical Research Center and School of Chemistry and Chemical Engineering, Southeast University, Nanjing 211189, PR China

Complete contact information is available at: <https://pubs.acs.org/10.1021/acs.jmedchem.1c00079>

Author Contributions

[§]Y.W. and X.W. contribute equally to this work.

Notes

The authors declare no competing financial interest.

ACKNOWLEDGMENTS

We would like to thank National Natural Science Foundation of China (Project no. 22077015), Fundamental Research Funds for the Central Universities (Project 2242020K30059), and Graduate Research and Innovation Fund of Jiangsu Province, China (Grant KYCX19_0102) for financial aid to

this work. Nanjing Biorn Life Science Co. Ltd is acknowledged for the *in vivo* tests.

ABBREVIATIONS

AKT, protein kinase; ALDH1A1, aldehyde dehydrogenase 1A1; A549, human NSCLC cell; A459/cDDP, resistant to cisplatin A549 cells; Bax, Bcl-2 associated X protein; Bcl-2, B-cell lymphoma-2 protein; cDDP, cisplatin; CK2, casein kinase 2; Clk2, cell division cycle-like kinase 2; CSC, cancer stem cell; DCHF-DA, 2,7-dichlorodi-hydrofluorescein diacetate; DCM, dichloromethane; DMEM, Dulbecco's modified Eagle medium; EGF, epidermal growth factor; β -FGF, β -fibroblast growth factor; FITC, fluorescein isothiocyanate isomer; GSK-3 β , glycogen synthase kinase-3 β ; HepG2, human liver hepatocellular cancer cell; HR-MS, high resolution mass spectrometry; ICP-MS, inductively coupled plasma-mass spectrometry; IC₅₀, the half maximal inhibitory concentration; LO2, human normal hepatocytes cell; MMP, mitochondrial membrane potential; MMP-7, matrix metalloproteinase 7; NMR, nuclear magnetic resonance; PARP, poly ADP-ribose polymerase; PBS, phosphate buffer saline; PC-3, human prostate cancer cell; PI, propidium iodide; qRT-PCR, quantitative real-time PCR; RF, resistant factor; ROS, reactive oxygen species; γ H2AX, phosphorylation of H2AX; RP-HPLC, reversed-phase high performance liquid chromatography; TMS, tetramethylsilane; T24, human bladder cancer cell; UV-vis, ultraviolet and visible spectrophotometry

REFERENCES

- (1) Herbst, R. S.; Morgensztern, D.; Boshoff, C. The Biology and Management of Non-Small Cell Lung Cancer. *Nature* **2018**, *553*, 446–454.
- (2) Liu, M.; Zhang, L.; Huang, Q.; Li, N.; Zheng, B.; Cai, H. Cost-Effectiveness Analysis of Ceritinib and Alectinib Versus Crizotinib in the Treatment of Anaplastic Lymphoma Kinase-Positive Advanced Non-Small Cell Lung Cancer. *Cancer Manage. Res.* **2019**, *11*, 9195–9202.
- (3) Siegel, R. L.; Miller, K. D.; Jemal, A. Cancer Statistics, 2016. *Ca-Cancer J. Clin.* **2016**, *66*, 7–30.
- (4) Pfister, D. G.; Johnson, D. H.; Azzoli, C. G.; Sause, W.; Smith, T. J.; Baker Jr, S.; Olak, J.; Stover, D.; Strawn, J. R.; Turrisi, A. T.; Somerfield, M. R. American Society of Clinical Oncology Treatment of Unresectable Non-Small-Cell Lung Cancer Guideline: Update 2003. *J. Clin. Oncol.* **2004**, *22*, 330–353.
- (5) Lopci, E.; Rossi, S. Tumor Metabolism and Prognostic Role of EZH2 in Non-Small Cell Lung Cancer. *Transl. Cancer Res.* **2017**, *6*, S982–S988.
- (6) Nagasaka, M.; Gadgeel, S. M. Role of Chemotherapy and Targeted Therapy in Early-Stage Non-Small Cell Lung Cancer. *Expert Rev. Anticancer Ther.* **2018**, *18*, 63–70.
- (7) Yeh, C.-T.; Wu, A. T. H.; Chang, P. M.-H.; Chen, K.-Y.; Yang, C.-N.; Yang, S.-C.; Ho, C.-C.; Chen, C.-C.; Kuo, Y.-L.; Lee, P.-Y.; Liu, Y.-W.; Yen, C.-C.; Hsiao, M.; Lu, P.-J.; Lai, J.-M.; Wang, L.-S.; Wu, C.-H.; Chiou, J.-F.; Yang, P.-C.; Huang, C.-Y. F. Trifluoperazine, an Antipsychotic Agent, Inhibits Cancer Stem Cell Growth and Overcomes Drug Resistance of Lung Cancer. *Am. J. Respir. Crit. Care Med.* **2012**, *186*, 1180–1188.
- (8) Prasetyanti, P. R.; Medema, J. P. Intra-Tumor Heterogeneity from a Cancer Stem Cell Perspective. *Mol. Canc.* **2017**, *16*, 41.
- (9) Pattabiraman, D. R.; Weinberg, R. A. Tackling the cancer stem cells - what challenges do they pose? *Nat. Rev. Drug Discovery* **2014**, *13*, 497–512.
- (10) Martins-Neves, S. R.; Cleton-Jansen, A.-M.; Gomes, C. M. F. Therapy-Induced Enrichment of Cancer Stem-Like Cells in Solid Human Tumors: Where do We Stand? *Pharmacol. Res.* **2018**, *137*, 193–204.

- (11) Tirino, V.; Desiderio, V.; Paino, F.; De Rosa, A.; Papaccio, F.; La Noce, M.; Laino, L.; De Francesco, F.; Papaccio, G. Cancer Stem Cells in Solid Tumors: An Overview and New Approaches for Their Isolation and Characterization. *Faseb. J.* **2013**, *27*, 13–24.
- (12) Wang, D.; Lippard, S. J. Cellular Processing of Platinum Anticancer Drugs. *Nat. Rev. Cancer* **2005**, *4*, 307–320.
- (13) Wang, Z.; Deng, Z.; Zhu, G. Emerging platinum(IV) prodrugs to combat cisplatin resistance: from isolated cancer cells to tumor microenvironment. *Dalton Trans.* **2019**, *48*, 2536–2544.
- (14) Apps, M. G.; Choi, E. H. Y.; Wheate, N. J. The State-of-Play and Future of Platinum Drugs. *Endocr. Relat. Canc.* **2015**, *22*, 219–233.
- (15) Galanski, M.; Jakupec, M.; Keppler, B. Update of the Preclinical Situation of Anticancer Platinum Complexes: Novel Design Strategies and Innovative Analytical Approaches. *Curr. Med. Chem.* **2005**, *12*, 2075–2094.
- (16) Imran, M.; Ayub, W.; Butler, I. S.; Zia-ur-Rehman, I. Photoactivated Platinum-Based Anticancer Drugs. *Coord. Chem. Rev.* **2018**, *376*, 405–429.
- (17) Czarnomysy, R.; Surazyński, A.; Muszynska, A.; Gornowicz, A.; Bielawska, A.; Bielawski, K. A Novel Series of Pyrazole-Platinum(II) Complexes as Potential Anti-Cancer Agents that Induce Cell Cycle Arrest and Apoptosis in Breast Cancer Cells. *J. Enzym. Inhib. Med. Chem.* **2018**, *33*, 1006–1023.
- (18) Galluzzi, L.; Senovilla, L.; Vitale, I.; Michels, J.; Martins, I.; Kepp, O.; Castedo, M.; Kroemer, G. Molecular Mechanisms of Cisplatin Resistance. *Oncogene* **2012**, *31*, 1869–1883.
- (19) Kelland, L. The Resurgence of Platinum-Based Cancer Chemotherapy. *Nat. Rev. Cancer* **2007**, *7*, 573–584.
- (20) Black, J.; Lopez, S.; Cocco, E.; Schwab, C.; English, D.; Santin, A. Clostridium Perfringens Enterotoxin (CPE) and CPE-Binding Domain (*c*-CPE) for the Detection and Treatment of Gynecologic Cancers. *Toxins* **2015**, *7*, 1116–1125.
- (21) Kalathur, M.; Toso, A.; Chen, J.; Revandkar, A.; Danzer-Baltzer, C.; Guccini, I.; Alajati, A.; Sarti, M.; Pinton, S.; Brambilla, L.; Di Mitri, D.; Carbone, G.; Garcia-Escudero, R.; Padova, A.; Magnoni, L.; Tarditi, A.; Maccari, L.; Malusa, F.; Kalathur, R. K.; Cozza, L.; Ruzzene, A. P. G.; Delaleu, M. N.; Catapano, C. V.; Frew, I. J.; Alimonti, A. A Chemogenomic Screening Identifies CK2 as a Target for Pro-Senescence Therapy in PTEN-Deficient Tumours. *Nat. Commun.* **2015**, *6*, 7227.
- (22) Purwin, M.; Hernández-Toribio, J.; Coderch, C.; Panchuk, R.; Skorokhyd, N.; Filipiak, K.; de Pascual-Teresa, B.; Ramos, A. Design and Synthesis of Novel Dual-Target Agents for HDAC1 and CK2 Inhibition. *RSC Adv.* **2016**, *6*, 66595–66608.
- (23) Hashimoto, A.; Gao, C.; Mastio, J.; Kossenkov, A.; Abrams, S. I.; Purandare, A. V.; Desilva, H.; Wee, S.; Hunt, J.; Jure-Kunkel, M.; Gabrilovich, D. I. Inhibition of Casein Kinase 2 Disrupts Differentiation of Myeloid Cells in Cancer and Enhances the Efficacy of Immunotherapy in Mice. *Cancer Res.* **2018**, *78*, 5644–5655.
- (24) Nitta, R. T.; Gholamin, S.; Feroze, A. H.; Agarwal, M.; Cheshier, S. H.; Mitra, S. S.; Li, G. Casein kinase 2 α regulates glioblastoma brain tumor-initiating cell growth through the β -catenin pathway. *Oncogene* **2015**, *34*, 3688–3699.
- (25) Pierre, F.; Chua, P. C.; O'Brien, S. E.; Siddiqui-Jain, A.; Bourbon, P.; Haddach, M.; Michaux, J.; Nagasawa, J.; Schwaebe, M. K.; Stefan, E.; Vialettes, A.; Whitten, J. P.; Chen, T. K.; Darjanian, L.; Stansfield, R.; Anderes, K.; Bliesath, J.; Drygin, D.; Ho, C.; Otori, M.; Proffitt, C.; Streiner, N.; Trent, K.; Rice, W. G.; Ryckman, D. M. Discovery and SAR of 5-(3-chlorophenylamino)benzo[*c*][2,6]-naphthyridine-8-carboxylic Acid (CX-4945), the First Clinical Stage Inhibitor of Protein Kinase CK2 for the Treatment of Cancer. *J. Med. Chem.* **2011**, *54*, 635–654.
- (26) Zhang, J.; Yang, P. L.; Gray, N. S. Targeting Cancer with Small Molecule Kinase Inhibitors. *Nat. Rev. Cancer* **2009**, *9*, 28–39.
- (27) Katoh, M. Networking of WNT, FGF, Notch, BMP, and Hedgehog Signaling Pathways During Carcinogenesis. *Stem Cell Rev.* **2007**, *3*, 30–38.
- (28) Schwind, L.; Schetting, S.; Montenarh, M. Inhibition of Protein Kinase CK2 Prevents Adipogenic Differentiation of Mesenchymal Stem Cells Like C3H/10T1/2 Cells. *Pharmaceuticals* **2017**, *10*, 22/1–22/12.
- (29) Nakagawa, M.; Fujita, S.; Katsumoto, T.; Yamagata, K.; Ogawara, Y.; Hattori, A.; Kagiya, Y.; Honma, D.; Araki, K.; Inoue, T.; Kato, A.; Inaki, K.; Wada, C.; Ono, Y.; Yamamoto, M.; Miura, O.; Nakashima, Y.; Kitabayashi, I. Dual Inhibition of Enhancer of Zeste Homolog 1/2 Overactivates WNT Signaling to Deplete Cancer Stem Cells in Multiple Myeloma. *Cancer Sci.* **2019**, *110*, 194–208.
- (30) Becherel, O. J.; Jakob, B.; Cherry, A. L.; Gueven, N.; Fusser, M.; Kijas, A. W.; Peng, C.; Katyal, S.; McKinnon, P. J.; Chen, J.; Epe, B.; Smerdon, S. J.; Taucher-Scholz, G.; Lavin, M. F. CK2 Phosphorylation-Dependent Interaction Between Aprataxin and MDC1 in the DNA Damage Response. *Nucleic Acids Res.* **2010**, *38*, 1489–1503.
- (31) Di Maira, G.; Brustolon, F.; Bertacchini, J.; Tosoni, K.; Marmiroli, S.; Pinna, L. A.; Ruzzene, M. Pharmacological Inhibition of Protein Kinase CK2 Reverts the Multidrug Resistance Phenotype of a CEM Cell Line Characterized by High CK2 Level. *Oncogene* **2007**, *26*, 6915–6926.
- (32) Zhou, B.; Ritt, D. A.; Morrison, D. K.; Der, C. J.; Cox, A. D. Protein Kinase CK2 α Maintains Extracellular Signal-regulated Kinase (ERK) Activity in a CK2 α Kinase-independent Manner to Promote Resistance to Inhibitors of RAF and MEK but Not ERK in BRAF Mutant Melanoma. *J. Biol. Chem.* **2016**, *291*, 17804–17815.
- (33) Loizou, J. I.; El-Khamisy, S. F.; Zlatanou, A.; Moore, D. J.; Chan, D. W.; Qin, J.; Sarno, S.; Meggio, F.; Pinna, L. A.; Caldecott, K. W. The Protein Kinase CK2 Facilitates Repair of Chromosomal DNA Single-Strand Breaks. *Cell* **2004**, *117*, 17–28.
- (34) Zhang, S.; Long, H.; Yang, Y. L.; Wang, Y.; Hsieh, D.; Li, W.; Au, A.; Stoppler, H. J.; Xu, Z.; Jablons, D. M.; You, L. Inhibition of CK 2 α down-regulates Notch1 signalling in lung cancer cells. *J. Cell Mol. Med.* **2013**, *17*, 854–862.
- (35) Iegre, J.; Brear, P.; De Fusco, C.; Yoshida, M.; Mitchell, S. L.; Rossmann, M.; Carro, L.; Sore, H. F.; Hyvönen, M.; Spring, D. R. Second-generation CK2 α inhibitors targeting the α D pocket. *Chem. Sci.* **2018**, *9*, 3041–3049.
- (36) Kim, H.; Choi, K.; Kang, H.; Lee, S.-Y.; Chi, S.-W.; Lee, M.-S.; Song, J.; Im, D.; Choi, Y.; Cho, S. Identification of a Novel Function of CX-4945 as a Splicing Regulator. *PLoS One* **2014**, *9*, No. e94978.
- (37) Pagano, M. A.; Bain, J.; Kazimierzczuk, Z.; Sarno, S.; Ruzzene, M.; Di Maira, G.; Elliott, M.; Orzeszko, A.; Cozza, G.; Meggio, F.; Pinna, L. A. The Selectivity of Inhibitors of Protein Kinase CK2: an Update. *Biochem. J.* **2008**, *415*, 353–365.
- (38) Zhao, J.; Gou, S.; Liu, F. Potent Anticancer Activity and Possible Low Toxicity of Platinum(II) Complexes with Functionalized 1,1-Cyclobutanedicarboxylate as a Leaving Ligand. *Chem.—Eur. J.* **2014**, *20*, 15216–15225.
- (39) Khoury, T.; Ademuyiwa, F. O.; Chandraseekhar, R.; Jabbour, M.; DeLeo, A.; Ferrone, S.; Wang, Y.; Wang, X. Aldehyde Dehydrogenase 1A1 Expression in Breast Cancer is Associated with Stage, Triple Negativity, and Outcome to Neoadjuvant Chemotherapy. *Mod. Pathol.* **2012**, *25*, 388–397.
- (40) Kaipio, K.; Chen, P.; Roering, P.; Huhtinen, K.; Mikkonen, P.; Östling, P.; Lehtinen, L.; Mansuri, N.; Korpela, T.; Potdar, S.; Hynninen, J.; Auranen, A.; Grénman, S.; Wennerberg, K.; Hautaniemi, S.; Carpen, O. ALDH1A1-related stemness in high-grade serous ovarian cancer is a negative prognostic indicator but potentially targetable by EGFR/mTOR-PI3K/aurora kinase inhibitors. *J. Pathol.* **2020**, *250*, 159–169.
- (41) Wang, J.; Wang, L.; Ho, C.-T.; Zhang, K.; Liu, Q.; Zhao, H. Garcinol From *Garcinia Indica* Downregulates Cancer Stem-Like Cell Biomarker ALDH1A1 in Nonsmall Cell Lung Cancer A549 Cells through DDIT3 Activation. *J. Agric. Food Chem.* **2017**, *65*, 3675–3683.
- (42) Morath, I.; Hartmann, T. N.; Orian-Rousseau, V. CD44: More than a Mere Stem Cell Marker. *Int. J. Biochem. Cell Biol.* **2016**, *81*, 166–173.

- (43) Li, Y.; Rogoff, H. A.; Keates, S.; Gao, Y.; Murikipudi, S.; Mikule, K.; Leggett, D.; Li, W.; Pardee, A. B.; Li, C. J. Suppression of Cancer Relapse and Metastasis by Inhibiting Cancer Stemness. *Proc. Natl. Acad. Sci. U.S.A.* **2015**, *112*, 1839–1844.
- (44) Chen, J.-J.; Cai, N.; Chen, G.-Z.; Jia, C.-C.; Qiu, D.-B.; Du, C.; Liu, W.; Yang, Y.; Long, Z.-J.; Zhang, Q. The Neuroleptic Drug Pimozide Inhibits Stem-Like Cell Maintenance and Tumorigenicity in Hepatocellular Carcinoma. *Oncotarget* **2017**, *8*, 17593–17609.
- (45) Hooshmand, K.; Asoodeh, A.; Behnam-Rassouli, F. GL-9 peptide regulates gene expression of CD44 cancer marker and pro-inflammatory cytokine TNF- α in human lung epithelial adenocarcinoma cell line (A549). *Mol. Cell. Biochem.* **2016**, *423*, 141–149.
- (46) Lipinski, C. A. Lead- and Drug-Like Compounds: the Rule-of-Five Revolution. *Drug Discov. Today Technol.* **2004**, *1*, 337–341.
- (47) Wang, Z.; Xu, Z.; Zhu, G. A Platinum(IV) Anticancer Prodrug Targeting Nucleotide Excision Repair to Overcome Cisplatin Resistance. *Angew. Chem., Int. Ed.* **2016**, *55*, 15564–15568.
- (48) Luczak, M. W.; Zhitkovich, A. Monoubiquitinated γ -H2AX: Abundant product and specific biomarker for non-apoptotic DNA double-strand breaks. *Toxicol. Appl. Pharmacol.* **2018**, *355*, 238–246.
- (49) Bonner, W. M.; Redon, C. E.; Dickey, J. S.; Nakamura, A. J.; Sedelnikova, O. A.; Solier, S.; Pommier, Y. γ H2AX and cancer. *Nat. Rev. Cancer* **2008**, *8*, 957–967.
- (50) Chapman, J. R.; Jackson, S. P. Phospho-dependent interactions between NBS1 and MDC1 mediate chromatin retention of the MRN complex at sites of DNA damage. *EMBO Rep.* **2008**, *9*, 795–801.
- (51) Tirino, V.; Desiderio, V.; Paino, F.; De Rosa, A.; Papaccio, F.; La Noce, M.; Laino, L.; De Francesco, F.; Papaccio, G. Cancer Stem Cells in Solid Tumors: an Overview and New Approaches for Their Isolation and Characterization. *FASEB J.* **2013**, *27*, 13–24.
- (52) Thapa, R.; Wilson, G. D. The Importance of CD44 as a Stem Cell Biomarker and Therapeutic Target in Cancer. *Stem Cell. Int.* **2016**, *2016*, 1–15.
- (53) Lu, Y.; Zhu, H.; Shan, H.; Lu, J.; Chang, X.; Li, X.; Lu, J.; Fan, X.; Zhu, S.; Wang, Y.; Guo, Q.; Wang, L.; Huang, Y.; Zhu, M.; Wang, Z. Knockdown of Oct4 and Nanog Expression Inhibits the Stemness of Pancreatic Cancer Cells. *Canc. Lett.* **2013**, *340*, 113–123.
- (54) Asadzadeh, Z.; Mansoori, B.; Mohammadi, A.; Aghajani, M.; Haji-Asgarzadeh, K.; Safarzadeh, E.; Mokhtarzadeh, A.; Duijf, P. H. G.; Baradaran, B. microRNAs in Cancer Stem Cells: Biology, Pathways, and Therapeutic Opportunities. *J. Cell. Physiol.* **2019**, *234*, 10002–10017.
- (55) Wang, W.; Yi, M.; Chen, S.; Li, J.; Zhang, H.; Xiong, W.; Li, G.; Li, X.; Xiang, B. NOR1 Suppresses Cancer Stem-Like Cells Properties of Tumor Cells via the Inhibition of the AKT-GSK-3 β -Wnt/ β -catenin-ALDH1A1 Signal Circuit. *J. Cell. Physiol.* **2017**, *232*, 2829–2840.
- (56) Cohen, P.; Goedert, M. GSK3 Inhibitors: Development and Therapeutic Potential. *Nat. Rev. Drug Discovery* **2004**, *3*, 479–487.
- (57) Mills, C. N.; Nowsheen, S.; Bonner, J. A.; Yang, E. S. Emerging Roles of Glycogen Synthase Kinase 3 in the Treatment of Brain Tumors. *Front. Mol. Neurosci.* **2011**, *4*, 47.
- (58) Huang, X.; Huang, R.; Gou, S.; Wang, Z.; Liao, Z.; Wang, H. Combretastatin A-4 analogue: A Dual-Targeting and Tubulin Inhibitor Containing Antitumor Pt(IV) Moiety with a Unique Mode of Action. *Bioconjugate Chem.* **2016**, *27*, 2132–2148.
- (59) Breckenridge, D. G.; Xue, D. Regulation of Mitochondrial Membrane Permeabilization by BCL-2 Family Proteins and Caspases. *Curr. Opin. Cell Biol.* **2004**, *16*, 647–652.
- (60) Jin, S.; Guo, Y.; Song, D.; Zhu, Z.; Zhang, Z.; Sun, Y.; Yang, T.; Guo, Z.; Wang, X. Targeting Energy Metabolism by a Platinum(IV) Prodrug as an Alternative Pathway for Cancer Suppression. *Inorg. Chem.* **2019**, *58*, 6507–6516.
- (61) Takada, K.; Kawamura, T.; Inai, M.; Masuda, S.; Oka, T.; Yoshikawa, Y.; Shibata, N.; Yoshikawa, H.; Ike, O.; Wada, H.; Hitomi, S. Pharmacokinetics of Cisplatin in Analbuminemic Rats. *Biopharm. Drug Dispos.* **1999**, *20*, 421–428.
- (62) Zhou, Q.; Peng, C.; Du, F.; Zhou, L.; Shi, Y.; Du, Y.; Liu, D.; Sun, W.; Zhang, M.; Chen, G. Design, Synthesis and Activity of BBI608 Derivatives Targeting on Stem Cells. *Eur. J. Med. Chem.* **2018**, *151*, 39–50.
- (63) Livak, K. J.; Schmittgen, T. D. Analysis of Relative Gene Expression Data Using Real-Time Quantitative PCR and the 2- $\Delta\Delta$ CT Method. *Methods* **2001**, *25*, 402–408.
- (64) Trott, O.; Olson, A. J. AutoDock Vina: Improving the Speed and Accuracy of Docking with a New Scoring Function, Efficient Optimization, and Multithreading. *J. Comput. Chem.* **2010**, *31*, 455–61.